REVIEW

Two-dimensionally patterned nanostructures based on monolayer colloidal crystals: Controllable fabrication, assembly, and applications

Xiaozhou Ye, Limin Qi*

Beijing National Laboratory for Molecular Sciences (BNLMS), State Key Laboratory for Structural Chemistry of Unstable and Stable Species, College of Chemistry, Peking University, Beijing 100871, China

Summary   Colloidal lithography based on monolayer colloidal crystals (MCCs) is a facile, inexpensive, efficient, and flexible nanofabrication approaches towards a wide variety of two-dimensionally (2D) patterned nanostructures with high controllability and reproducibility. This review gives a systematic overview on the recent advances in the controllable fabrication and assembly of 2D patterned nanostructures assisted by MCCs, with particular attention paid to the applications of the MCC-based nanostructures. First, the representative methods for the self-assembly of hexagonal-close-packed (hcp) MCCs and other complex MCCs are introduced. Next, the MCC-assisted fabrication (e.g., etching and deposition) of 2D patterned nanostructures at different two-phase (e.g., gas/solid, liquid/solid, and gas/liquid) interfaces is described, which is followed by a discussion on the MCC-assisted assembly from preformed nanoscale building blocks. Then, the novel properties and emerging applications of the 2D patterned nanostructures based on MCCs in various fields, such as photonics, plasmonics, SERS, antireflection, surface wetting, biological and chemical sensing, solar cells, photocatalysis, field emission, biomimetic fabrication, and other biological and electronic applications, are summarized. An outlook on future developments in this area is also provided.
© 2011 Elsevier Ltd. All rights reserved.

Introduction

Two-dimensionally (2D) patterned nanostructures, such as 2D ordered nanostructure arrays, surface-patterned nanostructures, and free-standing 2D patterned films, have attracted intensive interest because they exhibit unique pattern-dependent properties and show promising applications in a variety of technologically important areas including photonics, electronics, optoelectronic devices, biological and chemical sensing, surface wetting, and energy conversion [1,2]. It is highly desirable to develop effective nanopatterning techniques for the high-throughput and low-cost fabrication of large-area 2D patterned nanostructures with adjustable structural parameters. Up to now, many lithography methods for patterning surface at micro- and

* Corresponding author. Tel.: +86 10 62751722;
fax: +86 10 62751708.
    E-mail address: liminqi@pku.edu.cn (L. Qi).

nanoscale have been developed, such as photolithography, electron beam lithography, X-ray lithography, dip-pen lithography, nanoimprinting, and soft lithography [3—8]; however, they usually suffer from low throughput and high cost, or are limited by the prerequisite preparation of appropriate templates (e.g., masks, stamps, or molds). In this regard, surface-patterning methods employing templates prepared by self-assembly processes are highly efficient in fabricating 2D patterned nanostructures in large area since they are basically time-saving approaches with low equipment cost compared with the conventional lithography methods [2]. In particular, the fabrication and assembly approaches based on monolayer colloidal crystal (MCC) templates have turned out to be very effective and versatile routes towards functional 2D patterned nanostructures owing to their low lost, high throughput, high reproducibility, and easy controllability over the chemical composition and structural parameters [9—15].

Colloidal crystals are periodically ordered arrays of monodisperse colloidal particles (typically, micro- and nanospheres ranging from several micrometers to tens of nanometers in diameter), which represent a new class of self-assembled materials showing potential applications in many fields, such as photonic crystals, catalysis, sensing, and wetting [16—20]. In general, highly monodisperse colloidal microspheres or nanospheres can self-assemble into three-dimensional (3D) and two-dimensional (2D) colloidal crystals under appropriate conditions. While 3D colloidal crystals have drawn extensive attention owing to their practical applications as colloidal photonic crystals or as templates for fabricating 3D ordered macroporous (3DOM) materials, 2D colloidal crystals, which are monolayer arrays of colloidal particles or monolayer colloidal crystals, are attracting increasing interest because of their successful applications as versatile templates in surface patterning. The combination of MCC templates with different fabrication and assembly techniques results in a variety of MCC-based nanofabrication methods, which have been called ''natural lithography'' [21,22], ''nanosphere lithography'' [23,24], or ''colloidal lithography'' [9—11] in the literature. Such an MCC-based colloidal lithography has been recognized as a facile, inexpensive, efficient, and flexible nanolithography technique for fabricating functional 2D patterned nanostructures with a high reproducibility.

As the most frequently employed MCC templates in colloidal lithography, hexagonal-close-packed (hcp) monolayer colloidal crystals, which are monolayer arrays of hexagonally arranged, closely packed colloidal spheres, can be readily obtained by various interfacial self-assembly strategies [25]. Besides, non-close-packed (ncp) and patterned MCCs can be realized by many strategies including etching of hcp MCCs, spin-coating, electric-field-directed assembly, template-directed assembly, and transfer printing. The adjustability of the structural parameters of the MCCs, such as the sphere size, spacing, periodicity, and arrangement, enables the accurate control over the structural parameters of the resultant 2D patterned nanostructures. Moreover, deliberate combination with sophisticated fabrication and assembly techniques (e.g., etching, deposition, self-assembly, and transfer) affords more flexibility in tuning the structural parameters including feature size, shape, orientation, mutual distance, periodicity, and arrangement,

as well as desirable control of the chemical composition and materials properties of the final patterned nanostructures. Till now, the MCC-based colloidal lithography techniques have been successfully used for the controllable fabrication and assembly of a wide variety of 2D patterned nanostructures, such as 2D periodic arrays of various nano-objects (e.g., nanoparticles, nanotips, nanowires, nanobowls, nanovoids, nanorings, and nanocrescents), and free-standing nanonet films. It has been demonstrated that the 2D patterned nanostructures based on MCCs show great potential applications in many important areas, such as photonics, plasmonics, antireflection, surface wetting, biological and chemical sensing, solar cells, photocatalysis, field emission, and biomimetic fabrication.

In this review, we give a systematic overview on the recent advances in the controllable fabrication and assembly of 2D patterned nanostructures assisted by monolayer colloidal crystals, with particular attention paid to the applications of the MCC-based 2D patterned nanostructures. First, the representative methods for the self-assembly of hcp MCCs and other complex MCCs are introduced. Then, the MCC-assisted fabrication (e.g., etching and deposition) of 2D patterned nanostructures at different two-phase (e.g., gas/solid, liquid/solid, and gas/liquid) interfaces is described, which is followed a discussion on the MCC-assisted assembly from preformed nanoscale building blocks. Next, the novel properties and emerging applications of the 2D patterned nanostructures based on MCCs in various fields are summarized. Finally, conclusions and a short outlook on future developments are provided.

Self-assembly of MCCs

Hexagonal-close-packed MCCs

Hexagonal-close-packed (hcp) MCCs are the most commonly obtained and the most easily self-assembled MCCs since the hcp structure is the thermodynamically stable 2D arrangement of monodisperse isotropic colloidal spheres. The self-assembly methods of hcp MCCs are diverse and can be roughly divided into five typical strategies including drop-coating, dip-coating, spin-coating, electrophoretic deposition, and self-assembly at the gas—liquid interface, as illustrated in Scheme 1.

Nagayama and co-workers first observed the evaporation-induced convective assembly of randomly dispersed colloidal spheres into hcp MCCs by spreading a drop of dilute colloidal nanosphere suspension on a horizontal flat substrate [26]. During such a drop-coating procedure (Scheme 1a), the attractive capillary force and convective transport of the nanospheres arising from the continuous solvent evaporation are the main factors dominating the self-assembly process, and the ordering and quality of the obtained arrays are largely determined by the evaporation rate. Later on, Nagayama and co-workers developed a dip-coating procedure for continuous formation of hcp MCCs on a vertical flat substrate by accurately controlling the rates of water evaporation and substrate withdraw (Scheme 1b), resulting in centimeter-sized, polycrystalline MCCs [27]. Basically, the substrate can be inserted in the suspension at any tilted angles, and a slow and homogeneous
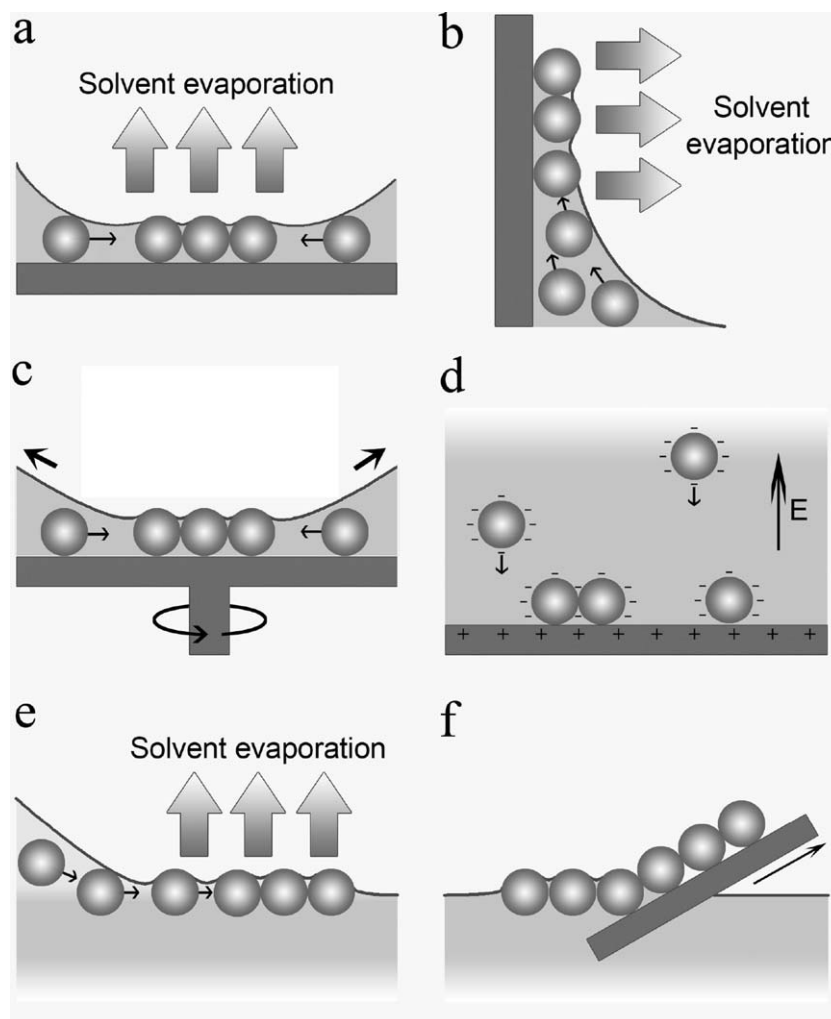
Scheme 1   Diverse self-assembly strategies towards hcp MCCs: (a) drop-coating, (b) dip-coating; (c) spin-coating; (d) electrophoretic deposition; (e) self-assembly at the gas/liquid interface; (f) transfer from the gas/liquid to the gas/solid interface.

evaporation is favorable for the formation of MCCs instead of multilayer colloidal crystals and improves the quality of the resulting MCCs. Under optimized conditions, large-scale, high-quality hcp MCCs can be controllably obtained via the dip-coating route albeit the assembly rate is relatively slow in most cases. For example, Fig. 1a shows a typical scanning electron microscopy (SEM) image of homogeneous hcp MCCs self-assembled from 560 nm silica spheres on a silicon wafer by dip-coating [28].

After the development of the dip-coating strategy, considerable efforts have been devoted to the improvement of the quality and productivity of the self-assembled MCCs, and thus some alternative strategies including spin-coating, electrophoretic deposition, and self-assembly at the gas—liquid interface have been developed. During spin-coating (Scheme 1c), the solvent flows across a wettable substrate at high shear rates, and the colloidal nanospheres are densely packed into hcp MCCs on the substrate rapidly. The quality and thickness of the resulting colloidal crystals are mainly affected by the spin speed, the concentration of the colloidal suspension, the rheology of the suspension, the wettability of the substrate, and the charges of the substrate

and nanospheres [29]. Because the spin-coating process is rapid and compatible with wafer-scale processes, the spin-coating methods have an advantage for both scaling-up and mass production. In electrophoretic deposition (Scheme 1d), a thin layer of colloidal suspension is confined between two electrodes, and an applied electrical field drives the charged nanospheres to move towards the electrodes, leading to their self-assembly into MCCs on the electrode interfaces. Electrophoretic deposition in direct current fields [30] or alternating current fields [31] has been applied for the rapid self-assembly and facile manipulation of MCCs because electrophoretic movement not only accelerates the sedimentation speed of nanospheres but also guides the growth of MCCs over a large area in a controlled manner.

Besides, self-assembly at the gas/liquid interface is a facile and efficient route towards large-area MCCs since nanospheres at the interface are able to exclusively form a monolayer without variation in the layer thickness, which is hardly realized in the evaporation-induced self-assembly on solid substrates. In a typical self-assembly at the gas/liquid interface (Scheme 1e), a colloidal suspension is spread onto a liquid surface through a spreading agent. After evaporation
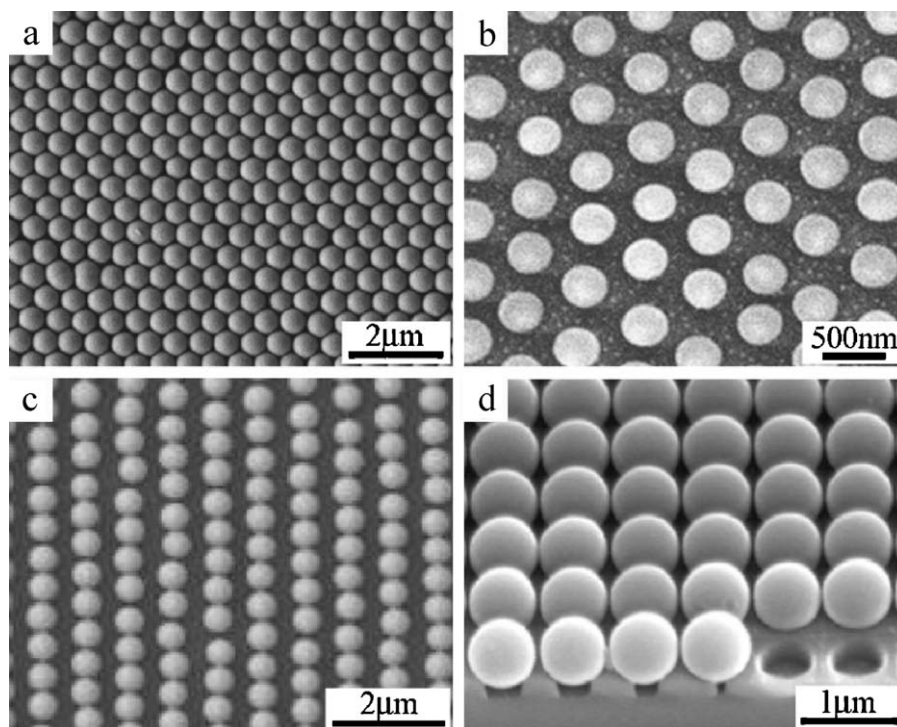
Figure 1 SEM images of MCCs with different patterns. (a) hcp MCCs of 560 nm silica spheres assembled by dip-coating. Reprinted with permission from Ref. [28]. Copyright 2010 American Chemical Society. (b) ncp MCCs of 315 nm silica spheres assembled by spin-coating. Reprinted with permission from Ref. [35]. Copyright 2006 American Institute of Physics. (c) Parallel lines of 566 nm silica spheres fabricated by stretching the PDMS film. Reprinted with permission from Ref. [38]. Copyright 2005 American Chemical Society. (d) Perfect square arrays of 700 nm silica spheres assembled by fitting into patterned nanowells. Reprinted with permission from Ref. [39]. Copyright 2009 American Chemical Society.

of the solvent of the suspension, the nanospheres self-assemble into a floating, highly ordered MCC over a large area. Colloidal nanospheres can be trapped at the gas/liquid interface as a result of the electrostatic and capillary forces or the surface hydrophobicity of the nanospheres [9]. After appropriately compressed, the resultant floating MCCs at the gas/liquid interface can be readily transferred onto various substrates, as shown in Scheme 1f. These processes can be favored by the well-established Langmuir—Blodgett technique [32]. There have been continuous efforts devoted to the modification of the self-assembly procedure at the gas/liquid interface, aiming at quickly obtaining large-area MCCs with enhanced quality and controllability. Recently, we developed an improved procedure for the self-assembly of large-area, high-quality hcp MCCs at the air/water interface [33]. A colloidal suspension was first dropped on the top of a cleaned horizontal glass slide, which was placed in the center of a Petri dish with its upper edge at the same level with the surrounding water. Then, the colloidal suspension spread freely to cover nearly the whole water surface, leading to the self-assembly of a floating high-quality hcp MCC within several seconds. After simple compression or consolidation by adding a surfactant solution onto the bare water surface, the floating hcp MCC was picked up by using an arbitrary substrate. As such, a uniform, high-quality, hcp MCC film as large as several square centimeters can be routinely obtained, which can be further used as easily processable templates for colloidal lithography.

Non-close-packed MCCs

For fully exploiting the application potential of MCCs as templates in colloidal lithography techniques, it is highly desirable to diversify the hcp MCCs into various non-close-packed (ncp) MCCs. Up to now, several fabrication strategies have been developed for the preparation of various ncp MCCs, including hexagonal ncp MCCs as well as patterned MCCs.

Hexagonal ncp MCCs can be naturally fabricated by etching highly ordered hcp MCCs. During the etching process, the diameters of the colloidal spheres are reduced while the interstice between the spheres is enlarged. By finely tuning the etching duration, rate and other conditions, the size, shape, and smoothness of colloidal spheres can be accurately controlled [34]. Besides etching, spin-coating and electric-field-directed assembly are also effective methods for the fabrication of hexagonal ncp MCCs. By spin-coating a colloidal dispersions of silica nanospheres on a flat substrate followed by polymerization, a well-defined hexagonal ncp MCC can be obtained, as shown in Fig. 1b [35]. By electric-field-directed assembly, charged colloidal nanospheres can self-assemble into hexagonal ncp MCCs under an alternate electro field (AEF), and the equilibrium distance of the nanospheres could be fine tuned by adjusting the parameter of the applied AEF [36].

In addition to the hexagonal ncp MCCs, patterned or complex ncp MCCs could also be obtained through

various assembling strategies, such as transfer printing and template-directed assembly. Yang and co-workers reported the fabrication of patterned MCCs on flat substrates by lift-up soft lithography, which is based on the selective transfer of a layer of MCC to the protruding surface of poly(dimethylsiloxane) (PDMS) elastomer stamp [37]. Utilizing the mechanical deformation behaviors of the PDMS elastomer, ncp MCCs with designable lattice structures on solid substrates can be easily obtained; for example, parallel lines of silica spheres were obtained by stretching the PDMS film (Fig. 1c) [38].

Alternatively, template-directed assembly is a very effective route towards complex ncp MCCs with designed patterns. Both topologically patterned substrates and chemically patterned surfaces can be used as the templates for surface patterning. By assembling colloidal nanospheres on delicately designed topologically patterned substrates, plenty of new and complex arrangement of colloidal nanospheres may be fabricated, which can hardly be achieved by simple self-assembly approaches. Recently, through the method of dry manual assembly on different templates, different types of MCC patterns include 1D wires, 1D strips, hexagonal arrays, and square arrays (Fig. 1d) were successfully fabricated [39]. On the other hand, assembly of colloidal spheres into 2D patterns can be realized on chemically patterned surfaces. The chemically patterned surface could result in preferential adsorption of colloidal nanospheres to the selected domains on the substrates, which are usually fabricated by modifying their surface with chemical functional units such as self-assembled membranes (SAMs) and other organic molecules [40]. In addition to electrostatic interaction and supramolecular interactions, DNA-mediated interactions can also be used for assembly of patterned MCCs. For instance, by producing spatial controllable DNA-surface patterns and DNA-functionalized polystyrene colloids, a sequence-specific reversible self-assembly of well-ordered MCCs with specific patterns was achieved recently [41].

Binary MCCs

Binary colloidal crystals are colloidal crystals assembled by two kinds of monodisperse colloidal particles (usually with different sizes). Binary colloidal crystals show rich arrays of crystal symmetries and different stoichiometries depending on the size ratio and concentration, compared to the limited crystal structures assembled by single-sized colloidal spheres. 2D binary colloidal crystals consisting of one monolayer of the larger spheres and one or more layers of the smaller spheres may be referred to as binary MCCs, which can be employed as unique 2D templates with rich patterns for colloidal lithography.

Some self-assembly methods have been developed to fabricate binary MCCs, and they can be roughly divided into two strategies: stepwise assembly and co-assembly. Based on stepwise assembly, van Blaaderen and co-workers developed a nonequilibrium layer-by-layer growth process and fabricated large-area binary MCCs for the first time [42]. This method seems versatile but has the limitation that it often takes quite a long time to form binary colloidal crystals. To overcome this limitation, a stepwise spin-coating was invented to allow rapid fabrication of binary colloidal crystals [43]. It is shown that the spin speed, as well as diameter radio, could affect the stoichiometry of the resulting binary colloidal crystals. This method realized the rapid fabrication of binary MCCs, but the stoichiometries of as-prepared binary MCCs are quite limited. Later on, several different stepwise assembly strategies, such as confined convective assembly [44] and sequential growth [45], are also employed, and provided a variety of stoichiometries of binary MCCs.

Co-assembly is an alternate approach to fabricate binary MCCs. Kitaev and Ozin reported an accelerated evaporation method to prepare binary MCCs with a rich variety of stoichiometries [46]. However, the fabrication process requires several hours. Recently, Yan and co-workers demonstrated an easy and fast process to fabricate large-area 2D binary MCCs by using a co-self-assembly approach at the air/water interface [47]. Taking advantage of the self-assembly at the gas/liquid interface, this method provides a simple, inexpensive, and fast route towards binary MCCs with adjustable stoichiometries.

Controllable etching assisted by MCCs

MCC-assisted etching, where MCCs are used as masks so that etching proceeds through the interstices between the colloidal nanospheres, is a simple and straightforward method to fabricate various 2D patterned nanostructures. Generally, it can be divided into two types: dry etching by reactive ions through reactive ion etching (RIE) and wet etching by etchants in solutions such as fluorine ions for silicone and silica.

Dry etching

Dry etching assisted by MCCs has been employed to fabricate various nanostructure arrays and nanonet films for the advantage of high controllability, high selectivity and the realization of anisotropic etching.

Nanopillar arrays can be easily fabricated by MCC-assisted dry etching process. Take Si nanopillar arrays as an example: a suspension of silica spheres was dip-coated on a silicon substrate to form hcp MCCs; then, by applying deep reactive ion etching with SF_6, the silica spheres were used as a mask and the area of substrate uncovered by silica spheres were etched; after removing the silica beads in HF, uniform periodic nanowire arrays of silicon were formed (Fig. 2a) [48]. The diameter and pitch of obtained nanowire arrays were determined by the diameter of silica spheres while the length of nanowires could be tuned by changing the etching time. Moreover, if the nanospheres were also etched during the process, only slower than the substrate, hydrogenated amorphous Si nanocone arrays instead of nanopillar arrays were obtained, which could function as both absorber and antireflection layers in solar cells [49]. In addition, by applying stepwise selective etching, some complex patterns of nanopillar arrays such as GaSb ''micro-candle stands'' could also be fabricated with the assistance of MCCs (Fig. 2b) [50].

Apart from nanopillar arrays, other 2D patterned nanostructures can also be obtained by MCC-assisted dry etching process. For instance, Using MCCs as lithographic masks,
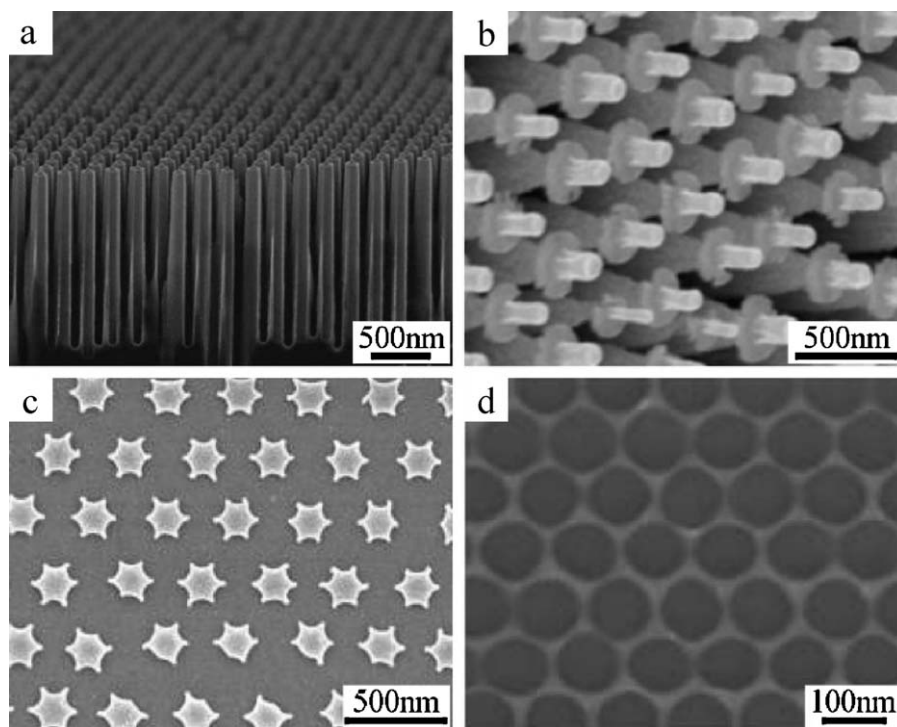
Figure 2 SEM images of patterned nanoarrays fabricated by dry etching. (a) Ordered silicon nanowire radial p—n junction arrays made by deep reactive ion etching. Reprinted with permission from Ref. [48]. Copyright 2010 American Chemical Society. (b) GaSb ''micro-candle stands'' made by stepwise selective etching. Reprinted with permission from Ref. [50]. Copyright 2008 The Royal Society of Chemistry. (c) PS nanostar arrays made by electron irradiation and subsequent heating of PS colloidal monolayers. Reprinted with permission from Ref. [52]. Copyright 2008 American Chemical Society. (d) Graphene nanomesh patterned using silica nanospheres by reactive ion etching. Reprinted with permission from Ref. [54]. Copyright 2010 American Chemical Society.

sub-100 nm triangular nanopore arrays with size and shape tunability were fabricated via angle-resolved reactive ion etching [51]. Through adjusting the etching condition and the size of nanospheres, nanoholes with in-plane widths ranging from 44 to 404 nm and depths ranging from 25 to 250 nm were fabricated. Notably, a novel route based on the electron irradiation of a polystyrene (PS) MCCs followed by thermal decomposition was developed for fabricating various nanoarrays with irregular units (Fig. 2c) [52]. Besides, by using spin-coated poly(ferrocenylmethylphenylsilane) (PFMPS) that inherited the MCC structure as etching resist, following the multilayer fabrication process, free-standing polyethersulfone (PES) nanonet films exhibiting regular arrays of circular holes with a high porosity were fabricated [53].

The fabrication of graphene nanostructures with feature sizes less than 10 nm has attracted considerable interest since they were shown to have electronic band gaps large enough for room temperature transistor operation theoretically and experimentally. Recently, dry etching process combing MCC templates was demonstrated to be a possible and controllable approach to fabricate such graphene nanostructures, such as patterned graphene nanomeshes (GNM) [54]. In a typical fabrication process, silica spheres were first assembled on a layer of graphene and slightly etched to form ncp MCCs. Then, a thin layer of metal was deposited on the substrates to act as etching mask during the following step and silica spheres were removed. Finally, reactive ion etching was used to remove the unprotected graphene, and large area GNM were prepared after removing the metal layer. Fig. 2d shows the SEM image of an as-prepared GNM that were obtained by masking graphene with 110 nm silica spheres, which demonstrated that narrow necks (<20 nm) in the GNM are attainable. More recently, Wang and co-workers fabricated ultranarrow graphene nanoribbons with the width of 12 nm, using a combination of MCC templates and low-power O_2 plasma etching [55]. The electrical properties of as-prepared structures were proved tunable by changing the widths of graphene nanoribbons.

Wet etching

Wet etching assisted by MCCs has also been employed to fabricate 2D patterned nanostructures by using strongly corrosive etchants in solutions. Compared with the dry etching, the wet-etching is more cost-effective although the applicable materials are rather limited.

The most commonly employed material in the MCC-assisted wet etching is silicone. In a typical fabrication of Si nanowire arrays, MCCs functioned as sacrificial masks to deposit metal nanoparticles in the voids of the nanospheres, and then the metal catalyzed the dissolution of the silicon beneath it during the etching process. The remnant silicon formed nanowire arrays with controllable diameter, length and density [56]. It was demonstrated that the used

wafer orientation would influence the alignment manner of Si nanowire arrays, and tilted Si nanowire arrays could be obtained on Si(1 1 1) substrates [57].

Notably, nanoring arrays could be fabricated via edge spread etching assisted by MCCs. The formation of self-assembled monolayers of thiol molecules on Au or Ag film could be guided by the edges of arrayed nanospheres, and the obtained pattern of SAMs is nanoring arrays around the nanospheres. Then, by wet etching the uncovered metal film after removing the colloidal beads, novel metal nanoring arrays were obtained [58].

Controllable deposition assisted by MCCs

MCC-assisted deposition is a very powerful technique to fabricate 2D patterned nanostructures of various functional materials. The methods of deposition are of great variety and can be divided into gas/solid interface deposition, liquid/solid interface deposition and gas/liquid interface deposition based on the position where the deposition occurs. By choosing proper deposition methods and adjusting deposition conditions, different kinds of 2D patterned nanostructures of almost any materials can be readily fabricated, enabling a full exploitation of their pattern-dependent properties and applications.

Gas/solid interface deposition

Through gas/solid interface deposition assisted by MCCs, materials can deposit on both the nanospheres and the exposed area of substrates, indicating that patterns can be formed on the nanospheres or the substrates. This method was first demonstrated by Deckman and Dunsmuir who deposited Ag on the MCC-coated substrates, and obtained microcolumnar arrays on the substrates by removing the nanospheres [22]. Since then, a great deal of nanoparticle arrays and nanocolumn arrays of various materials has been fabricated. Furthermore, vapor growth is also utilized to generate patterned nanostructures by catalytic deposition.

Deposition on the substrate where is uncovered by MCCs can form various nanoparticle arrays under different conditions. In particular, if the propagation direction of vapor is normal to the substrate, triangular nanoparticle arrays would be generated with hcp MCC masks. Fig. 3a exhibits the atomic force microscopy (AFM) image of the Ag nanoparticle arrays obtained by MCC-assisted deposition [24]. The nanoparticle size can be tuned by thorough control over the size of nanospheres and the thickness of metal film, while the shape of the nanoparticles can be further changed after deposition by laser irradiation [59] and annealing [60].

Moreover, by utilizing angle-resolved deposition, enormous variety of nanoparticle arrays with increasing flexibility becomes possible. By controlling the tilted angle θ and azimuthal angle Φ, Van Duyne and co-workers illustrated that the shape and interparticle spacing of the nanoparticle arrays can be systematically changed [61]. Furthermore, by rotating the substrate with MCC masks during angle-resolved deposition, large-area, high-quality split ring arrays were obtained (Fig. 3b) [62]. Besides, nanocrescent arrays [63], binary arrays [64], and other nanoparticle arrays were also obtained by angle-resolved deposition assisted by MCCs.

Instead of deposition on the uncovered substrates only, materials can also deposit around the nanospheres of MCCs and form other nanostructure arrays. For instance, Rothschild and co-workers fabricated $CaCu_3Ti_4O_{12}$ on the MCCs template substrates and formed macroporous films via pulsed laser deposition (PLD) [65]. Besides, hexagonal nonclose-packed (hncp) anatase TiO_2 nanorod arrays could be fabricated by pulsed laser deposition (PLD) on nanospheres of MCCs and annealing in air (Fig. 3c) [66].

Vapor growth process can also be used as an effective method to fabricate nanostructure arrays assisted by MCCs. For the growth of carbon nanotube (CNT) arrays, catalysts such as Fe, Co, or Ni were deposited on the substrate templated with MCCs. After removing the PS nanospheres and annealing, catalyst nanodot arrays were formed. Then the CNTs grew on each catalyst dot by the plasma-enhanced chemical vapor deposition (PECVD) method and formed aligned periodic arrays [67]. Recently, broccoli-like CNT arrays were fabricated through a combination of inverse MCC templates and vapor growth process, and the prepared arrays exhibited profound iridescence phenomena, which was originated from special optical characteristics of periodic nanostructures [68]. Beside CNT arrays, other nanowire arrays could also be fabricated by vapor growth process, such as Si nanowire arrays [69] and ZnO nanorod arrays [70]. For instance, large-area hexagonally patterned ZnO nanorod arrays were fabricated with tunable spacings and diameters, which also have uniform shape and length, good crystal quality, and vertical alignment on the substrate (Fig. 3d) [70]. In this work, 3-mercaptopropyltriethoxysilane molecules were added as a connection between Au catalyst and substrate. As a result, the catalyst particle pattern with tiny size dispersion and regular shape was obtained, which was the key factor for the successful growth of individually patterned ZnO nanorod arrays with tunable spacing and diameters.

Liquid/solid interface deposition

Liquid/solid interface deposition is a wide term including various reaction processes in solution, such as electrochemical deposition, electroless plating, solution/sol dipping deposition, solution growth, polymerization, and molecular deposition. Each of the reaction processes can be combined with MCC templates for the controllable fabrication of 2D patterned nanostructures.

Electrochemical deposition
Electrochemical deposition is a widely used and cost-effective method for the fabrication of various micro- and nanostructures. With the assistance of MCC templates, plenty of periodic nanostructures of functional materials can be fabricated through electrochemical deposition with multiform and tunable morphologies. Normally, MCCs are coated on a conductive substrate that functions as work electrode. During the electrochemical deposition, the nucleation of desired materials takes place at the interstitial sites between the nanospheres. The morphology of as-prepared structures can be adjusted by varying the electrodeposition condition or the MCC templates. Recently, Zeng et al. used deformed MCCs as templates to produce tailored ZnO nanorod/nanowire arrays (Fig. 4a), which
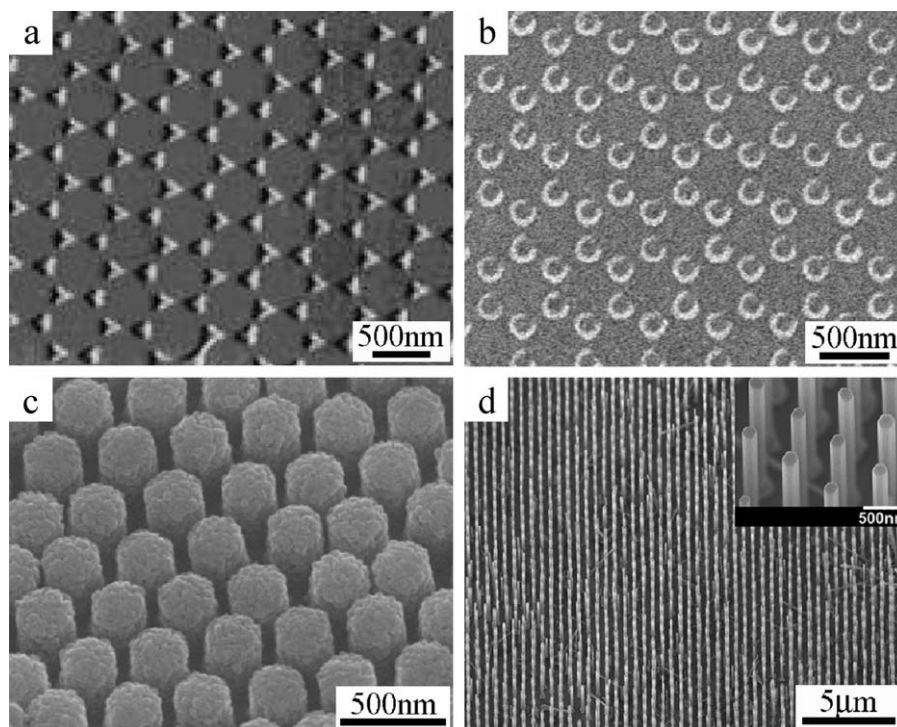
Figure 3   (a) AFM image of monolayer period Ag particle arrays by thermal evaporation using MCC templates with 542 nm nanospheres. Reprinted with permission from Ref. [24]. Copyright 2001 American Chemical Society. (b) SEM image of the periodic Au split ring resonator arrangement by angle-resolved deposition combining rotating the MCCs templates. Reprinted with permission from Ref. [62]. Copyright 2009 Wiley-VCH Verlag GmbH & Co. KGaA. (c) SEM image of a TiO$_2$ nanorod array by PLD using MCC templates with 350 nm nanospheres. Reprinted with permission from Ref. [66]. Copyright 2009 Wiley-VCH Verlag GmbH & Co. KGaA. (d) SEM images of periodic ZnO nanorod arrays by vapor growth using MCCs as templates. Reprinted with permission from Ref. [70]. Copyright 2009 The Royal Society of Chemistry.

exhibited considerable field-emission properties [71]. By adjusting the size and deformation of MCC templates and the choice of the electrolyte, the density, uniformity and tapering of the nanorod/nanowire arrays were all adjusted, leading to significant improvement of the field-emission performance of the arrays. It may be noted that the nucleation of the target material during electrochemical deposition can occur not only on the conductive substrate but also on the monolayer colloidal crystals. Elias et al. managed to make the nucleation take place on the PS spheres and the conductive substrate simultaneously and hence yielded hollow urchin-like ZnO thin film (Fig. 4b) [72]. The key mechanism for the nucleation on the PS surface is the treatment of them with ZnCl$_2$ at high concentration, which renders them electrically conductive. Apart from ZnO, periodic nanostructures of other materials including Ag [73] and Ni(OH)$_2$ [74] were also prepared via MCC-assisted electrochemical deposition.

Electroless plating
Electroless plating can deposit diverse metals by chemical reduction of dissolved metal ions, which can be used for the facile and inexpensive fabrication of various periodic nanostructures with the assistance of MCC templates. For instance, ordered array of gold nanoshells interconnected with gold nanotubes were fabricated via a combination of electroless plating and double templating (Fig. 4c) [75]. Specifically, a thin layer of gold thin film was deposited

on interconnect ncp MCCs, which were prepared by sintering and etching MCCs. After sealing the gold film in PS and removing SiO$_2$ nanosphere templates, gold was electroless-deposited on the void surface of the PS template and thus yielded the desired structures. Recently, Ahn and Roper discovered a novel technique to create regular arrays of spherical gold NPs on Si substrates by selective electroless plating [76]. The tuning of the shape and dimension of the produced nanostructures could be realized by controlling the availability of surface-associated water during silanization. This method allowed the reproducible fabrication of uniform metal nanoparticle arrays over large areas, which might possess potential applications in opto-plasmonic devices.

Solution/sol dipping deposition
The strategy of solution/sol dipping deposition assisted by MCC templates can obtain diverse ordered porous structured films of various metals, semiconductors and many other compounds on any substrates. The procedure is quite simple: a droplet of the precursor solution/sol is dropped onto substrates coated with MCCs firstly; upon drying the substrates, the solute precipitates or deposits on the substrates and the surface of colloidal nanospheres; after removal of MCC templates, ordered porous arrays are thus obtained. The morphology of porous films can be easily controlled by tuning the concentration of the precursor solution and
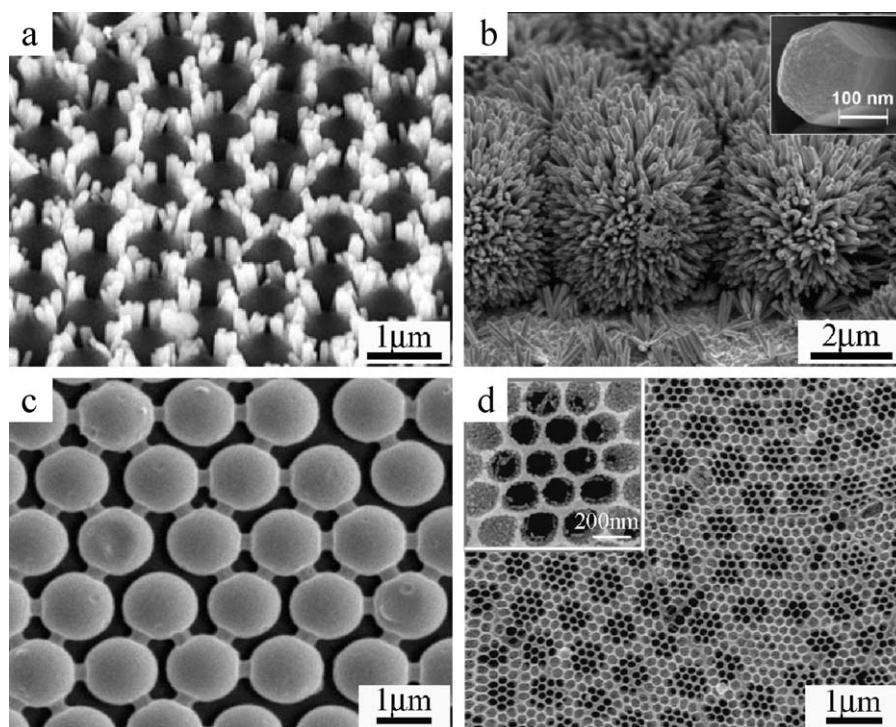
Figure 4   SEM image of patterned nanoarrays obtained by inorganic deposition at the liquid/solid interface. (a) Patterned ZnO nanorod arrays grown by electrochemical deposition from PS templates. Reprinted with permission from Ref. [71]. Copyright 2009 Wiley-VCH Verlag GmbH & Co. KGaA. (b) Ordered hollow urchin-like structure of ZnO nanowires fabricated by electrochemical deposition with PS templates. The inset is a high-magnification SEM image of the top of a nanowire grown at the top of the urchin-like structure. Reprinted with permission from Ref. [72]. Copyright 2010 Wiley-VCH Verlag GmbH & Co. KGaA. (c) 2D gold nanoshell/nanotube networks by electroless deposition. Reprinted with permission from Ref. [75]. Copyright 2006 Wiley-VCH Verlag GmbH & Co. KGaA. (d) In_2O_3 hierarchical porous structure obtained by solution dipping deposition. The inset is the local magnification. Reprinted with permission from Ref. [78]. Copyright 2009 American Chemical Society.

other treatment conditions [77]. Recently, In_2O_3 hetero-apertured micro/nanostructured ordered porous array was fabricated by this method using a layer-by-layer strategy (Fig. 4d) [78]. Two layers of MCCs with different sphere sizes were first assembled to form biperiodic ordered structures. After wetting such templates by floating them on the surface of precursor solution, drying, and annealing, In_2O_3 double-layer porous arrays were obtained, which exhibited remarkable gas sensing properties due to its high porosity.

Solution growth

Besides all the solution-based deposition methods mentioned above, MCC-assisted solution growth process is available for fabricating 2D patterned nanostructures with a high crystallinity and controlled crystal orientation. For instance, periodic bowl-like micropatterns of single crystal ZnO were prepared for the first time by solution-based epitaxial growth with the assistance of MCC templates [79]. It was proved that citrate anions were crucial to obtain the desired micropattern because they controlled the growth morphology. Recently, we developed a wet chemical approach to prepare hexagonally patterned arrays of well-aligned, regular ZnO nanopillars on zinc foils by MCC-assisted solution growth [33]. Two kinds of templates that were derived from MCC, i.e., inverted MCC (IMCC) and connected MCC (CMCC), were employed as masks to define

the growth sites and spaces on zinc foils for the realization of site-specific patterned growth of ZnO nanopillars, as shown in Scheme 2. The vertically aligned, well-crystallized ZnO nanopillars were also side-oriented, indicating a quasi-epitaxial growth on the zinc foils. Moreover, the width and spacing of the ZnO nanopillar arrays can be efficiently tuned by varying the aperture size of the templates and the reaction solution concentration.

Polymerization

Polymers are ideal candidates for structure replication since they do not adopt regular morphologies. By fulfilling MCCs with monomers and polymerizing afterwards, the absolute structure of MCCs would be replicated by polymers. By multistep replication or further deformation, different morphologies of polymers can be formed, which might exhibit special properties. For instance, by successive replica molding of PDMS and UV-curable photopolymer from the MCCs as the pristine template, close-packed microlens arrays were obtained [80]. Moreover, elliptical hemisphere arrays were fabricated by replicating stretched PDMS nanowell arrays, which is the replication of MCCs [81]. In addition to pure polymer nanostructures, polymer/inorganic composite nanostructures could also be prepared. Yang and co-workers fabricated large-area nanoring arrays of polystyrene, magnetite, Au, Si, magnetite nanoparticle/polystyrene and
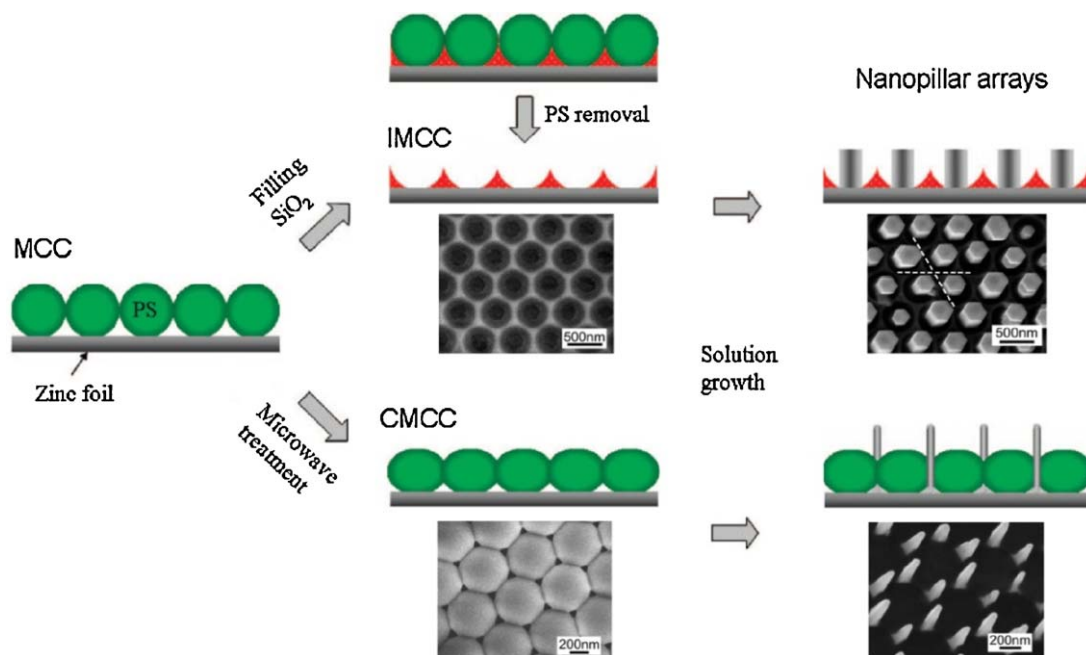
Scheme 2 Schematic illustration of the fabrication process of patterned ZnO nanopillar arrays using IMCC and CMCC templates. Reprinted with permission from Ref. [33]. Copyright 2009 American Chemical Society.

other composites by polymerization reaction assisted by monolayer colloidal crystal templates [82]. Recently, by combining the techniques of MCC templating, electropolymerization and polymer brush synthesis, topologically and chemically defined polymer surfaces with dual or binary composition patterns were successfully fabricated [83].

Protein deposition

The capacity to produce extended regions of nanopatterned protein on surfaces is of key importance across a number of chemically and biologically important applications including sensor development, proteomics and bioengineering. MCC templating combined with selective surface modification is an efficient and reliable route to realize the controllable assembly or deposition of protein molecules. For instance, Satriano and co-workers realized preferential immobilization of protein molecules by fabricating 2D hydrophilic/hydrophobic nanopore arrays [84]. Recently, binary colloidal crystals were also used as templates to fabricate tunable protein patterns. For example, N-heptylamine molecules were deposited through binary MCCs and formed patterned amine functionalized regions on substrates after plasma polymerization. Then, by grafting m-poly(ethylene glycol) propionaldehyde (m-PEG-PALD) on such amine functionalized regions, PEGylated surface areas that resisted nonspecific protein adsorption were obtained, and thus protein patterns were fabricated by depositing on the unmodified region [85]. In addition, highly ordered mixed protein patterns were fabricated using binary colloidal crystals as templates [86].

Gas/liquid interface deposition

Gas/liquid interface deposition employs floating MCCs at solution surface as the mask for the interfacial material deposition via reactions occurred at or near the gas/liquid interface, which provides a facile and efficient route towards free-standing patterned thin films. This method may be defined as colloidal lithography at the solution surface or nanosphere lithography at the gas/liquid interface.

The first gas/liquid interface deposition assisted by MCC templates was realized by Xu and Geodel using chemical polymerization at the air/water interfaces [87]. It was observed that MCCs could assist wetting of organic liquids on air/water interfaces and a uniform composite layer was thus formed. By polymerization reaction and removal of colloidal nanospheres, a free-standing porous polymer membrane with high uniformity of pores and pore ordering was synthesized. This membrane was further used to prepare gold nanoring arrays by solution dipping process [88]. Similarly, nanobowl arrays of conducting polymers were also fabricated by spreading colloidal crystal monolayer at the precursor aqueous solution/air interface [89]. During the polymerization process, the polymerized polymers were deposited on the hemisphere of the nanospheres submerging in the aqueous phase, thus forming nanobowl arrays of conducting polymers after removing MCC templates.

Photochemical reaction was also employed to fabricate inorganic nanostructure arrays via MCC-assisted gas/liquid interface deposition [90]. MCCs were floated on the surface of the precursor solution, and the crystal nuclei formed on the surfaces of nanospheres preferentially and grew subsequently during the photochemical reaction. As a result, free-standing nanobowl arrays were formed, which were composed of many small particles and hierarchical pores.

Recently, we developed a general approach towards free-standing patterned films based on the nanosphere lithography at the gas/liquid interface, which can be used for the facile fabrication of free-standing, high-quality nanonets and nanobowl arrays of various inorganic materials in a large scale via interfacial deposition assisted by
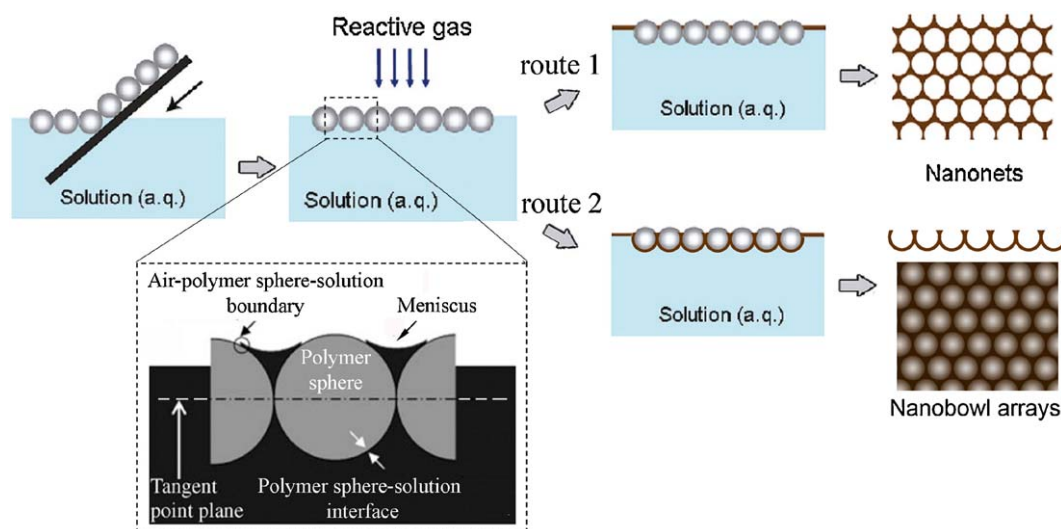
Scheme 3   Schematic illustration of the fabrication of nanonets and nanobowl arrays by nanosphere lithography at the gas/liquid interface.

MCCs [91—94]. The fabrication procedures are schematically illustrated in Scheme 3. Firstly, a pre-assembled MCC of polymer spheres was transferred onto the reactant solution surface. The solution can fill the triangular interstices among three adjacent polystyrene spheres under the action of capillary force, and the resulted meniscus lies above the tangent-point plane because of surface tension. Thus the air/polymer sphere/solution three-phase boundaries and the polymer sphere/solution interfaces around single spheres are formed. Then, a reactive gas is introduced and the material deposition occurs. If the nucleation process preferentially occurs at the gas/liquid interface, then free-standing nanonet are obtained after removing the polymer spheres (route 1); alternatively, if the nucleation process preferentially occurs at the liquid/solid interface, free-standing nanobowl arrays are obtained after removal of the polymer spheres (route 2).

As a typical example of nanonets, free-standing high-quality Ag_2S nanonets were facilely fabricated via the nanosphere lithography at the gas/liquid interface [91]. In this case, the reactant solution is aqueous $AgNO_3$ solution and the reactive gas is H_2S. As shown in Fig. 5a, the obtained Ag_2S nanonet film showing interesting photonic properties could be suspended freely on a copper grid with 0.1 mm-holes, which revealed its free-standing character. Fig. 5b shows an enlarged SEM image a nanonet film suspended on a silicon plate with terraces, confirming that the nanonet has a 2D flat net-like structure. The hole size, spacing, and film thickness of as-prepared nanonets could be easily tuned by adjusting MCC masks and reaction conditions. A free-standing nanonet folded during sample preparation is shown in Fig. 5c, which demonstrates its remarkable flexibility and therefore its compatibility with nonplanar surfaces. In addition, the excellent transferability of the present nanonets can be used to construct bilayer nanonets by a layer-by-layer method, which may be further used as the lithographic mask for metal deposition. Since the bilayer nanonets could be fabricated with different phase shifts, novel metal particle arrays with various patterns could be obtained, such

as a unique gold nanoleaf array in a triple-hexagonal order (Fig. 5d).

As a typical example of nanobowl arrays, free-standing 2D ordered macroporous (2DOM) Ag thin films were readily fabricated via the nanosphere lithography at the gas/liquid interface [92]. When the Ag^+ ions in the solution were reduced to form Ag nanoparticles, the nucleation preferentially occurred at the liquid/solid interfaces heterogeneously, hence the deposition of Ag occurred mostly at the lower surface of the spheres immersed in the $AgNO_3$ solution and at the triangular interstices among every three neighboring spheres. The SEM images of as-prepared Ag nanobowl arrays or 2DOM Ag thin film are shown in Fig. 6. The vertical top views of the obverse side show highly ordered hexagonally arranged circular macropores with a long-range periodicity, and obvious triangular top surface that duplicates the interspace among colloidal spheres (Fig. 6a and b). The tilted top views further verify the bowl-array-like, ordered macroporous structures and clearly show the triangular top surface (Fig. 6c and d). The obtained 2DOM Ag thin films exhibited typical properties of plasmonic crystals with vivid reflection colors on the obverse side. In addition, the facile fabrication of honeycomb-patterned thin films of amorphous calcium carbonate and mosaic calcite was achieved via the nanosphere lithography at the gas/liquid interface [93].

Controllable assembly assisted by MCCs

MCCs can not only be used as templates to assist controllable etching and deposition, but also be used as templates to direct the assembly of preformed nanoscale building blocks or nano-objects into hierarchical structures with periodic 2D patterns. Till now, MCC-assisted assembly of various nano-objects including nanospheres, carbon nanotubes, and PbS nanostars has been realized by different assembly strategies.
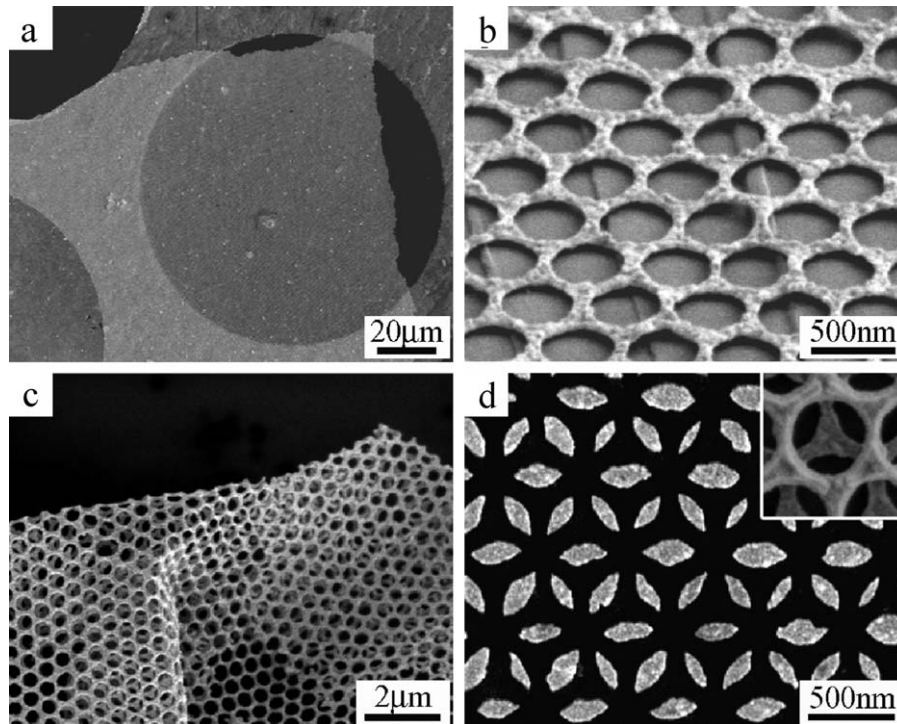
Figure 5 SEM images of Ag$_2$S nanonets suspended on a holey copper grid (a) and on a silicon plate with terraces (b), and a free-standing, folded nanonet (c). (d) SEM image of gold nanopatterns created by evaporation deposition with bilayer Ag$_2$S nanonets (inset) as the deposition masks.
Reprinted with permission from Ref. [91]. Copyright 2009 American Chemical Society.
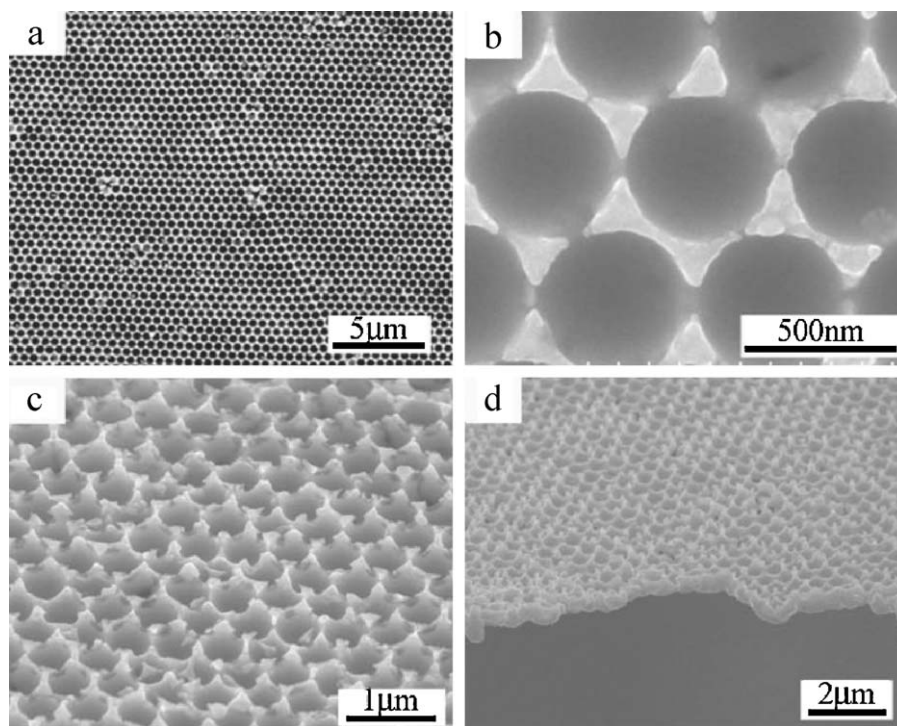
Figure 6 SEM images of 2DOM Ag thin film with a periodic spacing of 450 nm: (a, b) vertical top view; (c, d) tilted top view.
Reprinted with permission from Ref. [92]. Copyright 2010 Wiley-VCH Verlag GmbH & Co. KGaA.
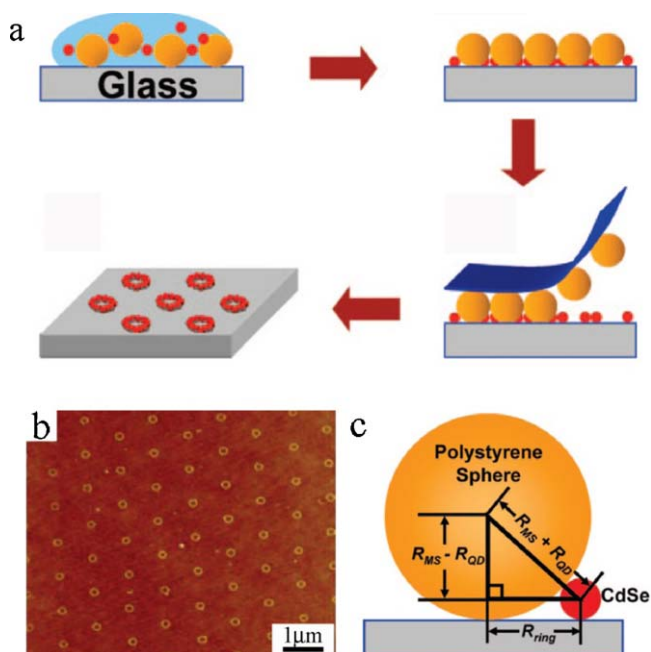
Figure 7   (a) Schematic diagram of the evaporation templating procedure employed for forming CdSe nanorings (red particles) on planar substrates using PS microsphere templates (orange particles). (b) AFM topographical image of CdSe nanorings formed with 1 μm PS spheres. (c) Schematic diagram of the hard sphere contact model employed for calculating the contact radius of the CdSe nanorings.
Reprinted with permission from Ref. [96]. Copyright 2009 American Chemical Society.

Assembly of nanospheres

The assembly of spherical particles, such as quantum dots (QDs) and gold nanoparticles, are wildly researched because it not only shows great potential applications in photonics, electronics, and sensing, but also serves as platforms for fundamental studies. Mulvaney and co-workers demonstrated a facile approach to assemble quantum dots into 2D arrays with the assistance of MCCs [95]. The process can be divided into three major steps: (i) Ag nanoparticle arrays were fabricated by gas/solid interface deposition assisted by MCCs; (ii) an SAM of a chemical linker was absorbed on the Ag nanoparticle arrays; (iii) core—shell CdSe@ZnS QDs with tunable luminescence were deposited on the SAM and thus form 2D arrays. Besides nanoparticle arrays, nanoring arrays of QDs could be fabricated by evaporation-induced assembly (Fig. 7) [96]. As illustrated in Fig. 7a, aqueous solution containing both colloidal nanospheres and CdSe QDs were dropped on to the hydrophilic surface coated by MCCs; then, during the evaporation, the nonvolatile QDs were driven to assemble at the PS/substrate interface by capillary forces, and finally formed nanoring arrays (Fig. 7b). The radius of as-prepared nanorings could be calculated using a simple hard sphere contact model (Fig. 7c). It was clear that the radius of the nanorings was determined by the diameter of colloidal spheres and QDs. Besides, the height and thickness of nanorings could be tuned by changing the size of colloidal nanospheres and the concentration of QDs.

Assembly of carbon nanotubes

The assembly of carbon nanotubes into networks or arrays has received great attention for their potential applications in the area of transparent conducting materials. A suspension containing colloidal spheres and CNTs were used for confined convective assembly of CNTs assisted by MCCs, during which the colloidal spheres were assembled into hcp MCCs and the CNTs were deposited onto the edge of the colloidal spheres, winding around them, because of the capillary forces and the high flexibility of CNTs [97]. By selectively removing the colloidal spheres, CNT films that have ordered network structures with regular voids were produced, which is highly conductive and transparent due to its sufficient densities and periodic structures. Besides CNTs networks, CNTs nanoring arrays with tunable ring diameters could also be fabricated by evaporation-induced assembly with the assistance of MCCs [98]. By dropping supernatant solution of single-walled carbon nanotubes (SWNTs) on MCCs templates, the liquid retracts towards the bottom of the spheres during evaporation, leading to the formation of ordered CNTs nanoring arrays.

Assembly of PbS nanostars

Despite remarkable success in the self-assembly of spherical nanoparticles, the realization of controllable self-assembly of nonspherical nanoparticles is still challenging. In this regard, MCCs provide a desired template for the directed assembly of well-defined PbS nanostars with six symmetric horns. Recently, the controllable assembly of monodisperse PbS nanostars into novel ncp arrays was achieved by evaporation-induced self-assembly assisted by MCC and IMCC templates [99]. The fabrication of ncp arrays of PbS nanostars via vertical deposition assisted by MCC and IMCC is illustrated in Scheme 4. With the MCC template (Scheme 4a), the vertical deposition resulted in the formation of ncp array of PbS nanostars with three horns stably standing on the template (denoted as ncp array-1). The voids among the neighboring colloidal spheres are the most stable positions for the deposition of PbS nanostars with three horns standing and the spacing between two neighboring nanostars was 130 nm, as precisely predefined by the MCC template. Considering that the PbS six-horn star is actually a single crystal with the six horns grown along the $\langle 1 0 0 \rangle$ directions and it uses three $\langle 1 0 0 \rangle$-oriented horns to stand on the template, ncp array-1 can be regarded as $[1 1 1]$-oriented assemblies; namely, the $[1 1 1]$ axis of the crystal is perpendicular to the plane of the template. On the other hand, with the IMCC template (Scheme 4b), patterned assemblies of $[0 0 1]$-oriented PbS nanostars with a single horn vertically standing on the template plane (designated as ncp array-2) can be fabricated. It is noteworthy that the height of the IMCC templates was considerably higher than the colloidal sphere equators, which resulted in relatively deep cavities with narrow necks. In this case, each nanostar was strictly oriented with a single horn inserted into the circular gap of the IMCC template and the opposite horn stretched
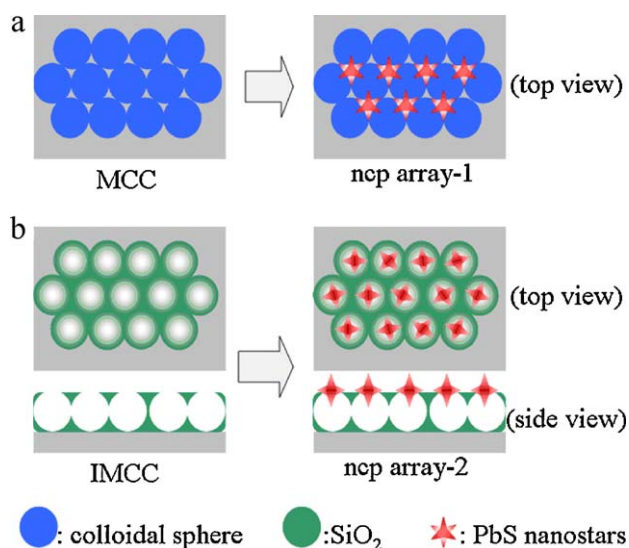
Scheme 4 Schematic illustration of the fabrication of ncp arrays of six-horn PbS nanostars assisted by MCC (a) and IMCC (b) through vertical deposition.
Reprinted with permission from Ref. [99]. Copyright 2010 American Chemical Society.

vertically upward. This MCC-assisted assembly strategy is a versatile approach and may open a new route for the controlled assembly of anisotropic nanostructured materials into large-scale ordered arrays with desirable patterns.

Properties and applications of MCC-based nanostructures

Optical properties

The inherent 2D periodicity ranging from tens of nanometers to several micrometers in the 2D patterned nanostructures based on MCCs endow them a rich variety of interesting optical properties related with photonic crystals [16,17], plasmonic crystals [100], plasmonic—photonic crystals [101], and patterned surfaces. In particular, photonic band gap, structural color, antireflection, surface plasmon resonance (SPR), and surface-enhanced Raman scattering (SERS) properties of the MCC-based nanostructures have attracted significant interest in recent years.

Photonic band gap and structural color
MCCs and the 2D patterned nanostructures constructed from them exhibit intriguing photonic band gap properties originating from the periodic variation of dielectric constant. Such properties have received great attention for the ability of controlling and manipulating the propagation of light and thus promising applications in photonic device engineering.

Since the position of the photonic band gap is associated with dielectric environment and lattice constant, the factors influencing those values will affect the position of the stop band. For instance, Li and co-workers fabricated 2D arrays of ZnO shells using MCC templates and investigated the optical characteristics of the as-prepared large-scale ordered arrays of ZnO hollow half-shell structures [102]. The ZnO half-shell

arrays with various shell thicknesses and nanosphere sizes were prepared and their transmission spectra were measured. As the shell thickness was increased from 110 nm to 260 nm, the band gaps red-shifted from 500 nm to 540 nm due to an increase in the average refractive index. With increasing the sphere size under the same ZnO shell thickness, the band gaps shifted to longer wavelength as well due to the increase of lattice constant. Similar results were also obtained from Ni(OH)$_2$ hollow sphere arrays, which were prepared by MCC-assisted electrochemical deposition [74]. By controlling the size of the PS spheres and changing the deposition time to adjust the shell thickness, the optical transmission stop band could be controlled in a large region. We also observed that the transmission spectra of the Ag$_2$S nanonets prepared with MCCs showed sharp transmission dips corresponding to the photonic band gaps, and there existed a linear relationship between the band gap and the periodicity of the nanonets [91]. Such tunable band gap properties of 2D periodic structures have great potential both in applications and in fundamental research, which is worthy of further investigation.

As a result of photonic band gap properties, many 2D ordered nanostructure arrays exhibit intensive structural colors. Recently, it was reported that even carbon nanotubes, an extremely dark materials due to their low reflection and high adsorption, displayed iridescent color when they were fabricated into patterned nanostructures [68]. It was proposed that the colorful images arose from the diffraction of light from the periodical array of CNTs. Further investigation indicated that the diffraction peaks shifted to longer wavelengths upon increasing the detection angle or the lattice constant, which agreed well with the theoretical values. The iridescence of patterned CNT arrays could find applications in various flexible devices, such as solar cells and displays.

Antireflection
The antireflective structures (ARS) are some sorts of patterned arrays that can suppress the reflection losses and increase transmission of light at the interface over a large range of wavelength. It has been discovered that the nipple arrays of nocturnal insects are typical antireflective structures. In practical applications, the ARS surfaces are of significant importance in the area of optical and electro-optical devices, and various efforts have been made to fabricate antireflective structures with improved antireflection properties [103]. In this regard, MCC-based nanostructures are ideal candidates for the high-performance ARS surfaces.

Nanopillar arrays are similar with the nipple arrays of those nocturnal insects, and thus exhibit profound antireflection properties. Using MCCs as templates, plenty of nanopillar arrays of various materials have been fabricated for antireflection applications. For instance, silicon nanopillar arrays with high aspect ratio were fabricated by using silica MCCs assembled on silicon wafer as etching mask. As the etching rate of silica is lower than that of silicon, the uncovered area of silicon substrates was etched and thus pillar arrays were directly formed on the silicon surface after removing MCC templates [104]. The as-prepared nanopillar arrays exhibit low reflection (<2.5%) over the whole visible-near-IR spectrum, indicating broadband antireflection. In

comparison, the bare wafer exhibited >30% reflectivity for all the wavelengths.

In order to promote the antireflective properties of the ARS surfaces, considerable efforts have been made to improve the morphologies of the ARS surfaces. Specifically, Cui and co-workers fabricated a-Si:H nanocone arrays through RIE process assisted by MCCs, which is shown in Fig. 8a [49]. Fig. 8b shows photographs of three different samples: a-Si:H thin film, nanowire arrays, and nanocone arrays with the same height as the film thickness. It is obvious that the thin film is mirror-like, the nanowire array reflects less light, and the nanocone array is the darkest one, exhibiting the strongest absorption due to suppression of reflection. The absorption spectrum measurement confirmed that nanocone arrays exhibit the highest absorption (98.4%) compared with nanowire arrays (85%) and thin film (75%) around normal incidence. It was proposed that the nanocone arrays provided a gradual reduction of the effective refractive index between air and the a-Si:H substrate, hence exhibiting superior antireflective properties compared with nanowire arrays. Later on, double-side nanocone array was fabricated with enhanced antireflective properties compared with planar surface and single-side nanocone array (Fig. 8c) [105]. As shown in Fig. 8d, the clear words below the double-side ARS surface demonstrated light-quality transparency and little reflection loss (top), while the planar silica substrate reflected sunlight (bottom). The antireflective properties of the double-side nanocone arrays were not sensitive to increase in the incidence angle but the reflection of single-side nanocone arrays increased when the incidence angle was increased.

In conclusion, many ARS surfaces with high performance were fabricated using MCC templates but the properties were not fully optimized yet. The fabrication of low-cost, high-performance, multifunctional ARS surfaces is still a meaningful goal to pursue and such ARS surfaces would find more applications in solar cells, shielding coatings and other areas.

SPR

Noble metal nanostructure arrays have pronounced surface plasmon resonance, which results from incident electromagnetic radiation exciting coherent oscillations of conduction electrons near a metal-dielectric interface [106]. At present, the SPR properties of such noble metal nanostructure arrays, which are highly dependent on the size, shape, lattice constants and dielectric environment, have attracted a great deal of attentions owing to their unique optical properties to route and manipulate light at nanometer length scales and hence important applications in many fields from biosensing to nanophotonics [107].

Localized surface plasmon resonance (LSPR), which is one of the SPR modes and is localized around the objects being excited, could generate locally enhanced electromagnetic field and have high intensities and spatial resolution. Nanostructure arrays with various geometries have been fabricated with the assistance of MCCs to reveal their tunable LSPR properties. For instance, Van Duyne and co-workers presented a systematically study of nanoparticle size, shape, interparticle spacing, solvent, and other relevant parameters on the LSPR of Ag nanoparticle arrays fabricated by MCC-assisted deposition [24]. According to their experimental results, the absorption band of the Ag nanoparticle arrays could be easily tuned from visible to the NIR range by tuning the fabricating condition. Recently, some special nanostructure arrays of asymmetric geometry such as crescent-shaped nanohole or nanoparticle arrays have been prepared and their interesting LSPR properties have been observed. Because of the asymmetric geometry and the existence of sharp tips, the crescent-shaped nanoholes showed special LSPR properties compared with other symmetric structures, such as significant polarization dependence and higher local field enhancement [108].

Beside LSPR, there is another SPR mode termed as delocalized SP, which is caused by multiple scatter of the periodic components of the array and only propagates in a short distance. By tuning the geometry parameters of nanostructure arrays, a transition from LSPR to delocalized SP can be clearly observed. Wang and co-workers fabricated ordered metallic microstructure by depositing a thin layer of Au onto MCCs [109]. By tuning the thickness of the deposited Au film, a geometrical transition from isolated hemispherical metal shells to an interconnected periodic metal network was achieved. For a sufficiently low thin metal layer, light scattering by the 2D dielectric periodic structure dominates the transmission spectra. When the gold deposit is increased, a continuous layer (nanocaps) may be formed on each silica sphere but no connection between each cap is formed. In such cases, localized surface plasmon polaritons (SPPs) can be excited and leads to the first strong redistribution of the photonic modes of the 2D dielectric photonic crystal. As the gold deposit is further increased, upon the formation of gold nanobridges between touching silica spheres, a transition from localized SPPs to extended SPPs occurs and gives rise to very high transmittance at specific wavelengths. Since the delocalized is highly relevant with periodicity of nanostructure arrays, they could be tuned by changing the lattice constant of periodic nanostructure arrays. For instance, By applying MCC-assisted deposition and transfer-printing technique, a monolayer array of Ag-capped PS spheres on an elastic PDMS substrate can been fabricated [110]. By mechanically stretching the PDMS substrates, the lattice type and the distance between neighboring Ag caps were both changed, either of which would strongly affect the coupling of surface plasmons between neighboring Ag caps, and finally lead to large shift of SPR and color change.

SERS

The surface enhanced Raman scattering is a powerful technique for sensitive and selective detection, which rests in the use of roughened, coinage metal surfaces to amplify scattering [111]. Many efforts have been paid to fabricate roughened metal films aiming at enlarging enhancement factors; however the full utility of SERS has not yet been realized with these substrates because of the poor stability and reproducibility. Recently, the low-cost fabrication of more precisely defined metal nanostructure arrays with high fidelity and high control is pursued with the assistance of MCCs because these structures may provide more reliable performance while still leading to reasonably large SERS enhancement factors.
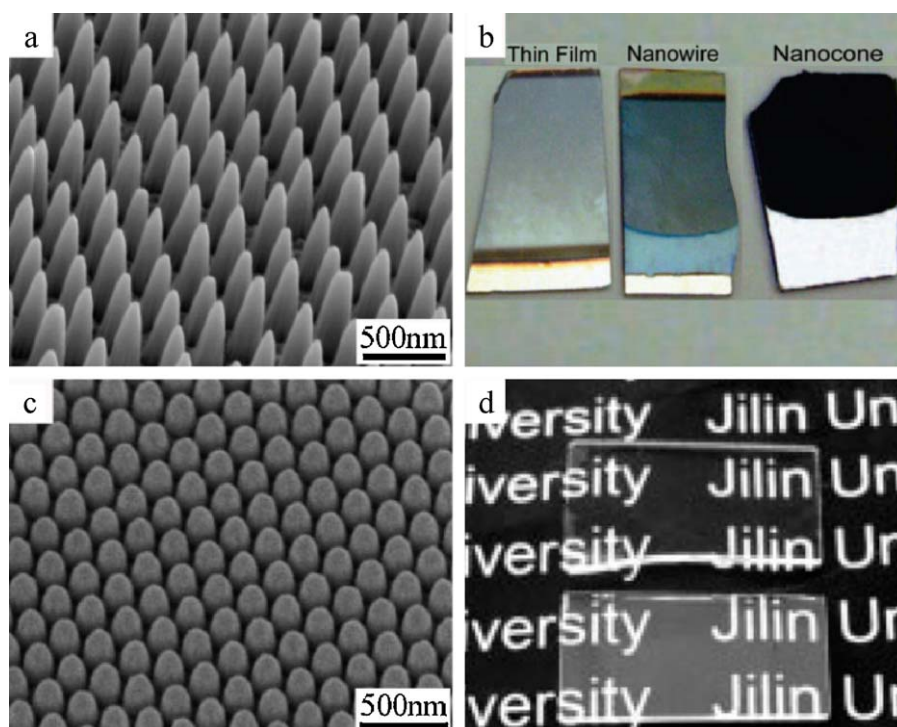
Figure 8 (a) SEM image of antireflective a-Si:H nanocone arrays. (b) Photographs of a-Si:H thin film (left), nanowire arrays (middle), and nanocone arrays (right). Reprinted with permission from Ref. [49]. Copyright 2009 American Chemical Society. (c) SEM image of ARS surfaces made of silica cone arrays. (d) Photographs of double-sided ARS surfaces (up) and planar silica substrate (down).
Reprinted with permission from Ref. [105]. Copyright 2009 Wiley-VCH Verlag GmbH & Co. KGaA.

Fang et al. fabricated Ag film on nanospheres as SERS substrates and measured the distribution of site enhancements [112]. They demonstrated the existence of ''hot spots'' and the great contribution to the whole SERS signal from a few amount molecules at hot spots. Recently, Farcau and Astilean confirmed the site of hot spot on Au film-on-nanospheres substrate through mapping and demonstrated that the mostly enhanced electromagnetic (EM) field is confined at the edges and sharp crevices between adjacent metallic half-shells [113]. Besides the metal films on MCCs, metal nanobowl arrays templated by MCCs can also be employed as effective SERS substrates. Bartlett and co-workers fabricated Pd and Pt nanobowl arrays by MCC-assisted electrodeposition, and reproducible surface enhancements for Raman scattering was obtained by tuning the film thickness and sphere diameters [114]. Moreover, Ag nanobowl arrays obtained by nanosphere lithography at the gas/liquid interface showed SERS enhancement factors as high as the 10^7 order, which made them a promising sensor for the detection of trace amount of analyte adsorbed on the surface [92].

It is known that the spatial confinement of small molecules near hot spots is essential for the SERS detection of small molecules at low concentration. In a recent work, Jeong and co-workers presents the SERS enhancement of small molecules spatially entrapped near electromagnetic hot spots by using nanofluidic channels with plasmonic nanostructures based on MCCs [115]. As shown in Fig. 9, a monolayer of silver film over MCCs of silica nanospheres (AgFONs) is prepared on a glass substrate and covered by a PDMS slab. Small molecules are introduced into the interstitial nanogaps between AgFONs and PDMS, which serve as ''nanofluidic channels''. The nanofluidic channel has an assortment of stagnation points near the cuspidal points between contiguous nanospheres, where the diffused small molecules are spatially confined and concentrated. The concurrence between nanofluid stagnation points and electromagnetic hot spots significantly increases the SERS signals due to a large number of small molecules placed near hot spots.

Wettability

The wettability of solid surfaces is an important property depending on both chemical compositions and the surface structure. Generally, the wettability is associated with the surface roughness for a certain material. A great number of ordered arrays based on MCCs are rough on the micro-/nanoscale and could induce different wettabilities. For instance, large-scale ordered silica pore arrays with mesoporous skeletons were fabricated by the MCC-assisted sol—gel technique, and such specially structured silica demonstrated superhydrophilicity with a water contact angle (CA) of 5° and superhydrophobicity with a water CA of 154° before and after surface modification with fluoroalkylsilane, respectively [116]. Recently, Koshizaki and co-workers fabricated vertically ordered Co_3O_4 hierarchical nanorod arrays using pulsed laser deposition (PLD) followed by an annealing process, and the as-prepared Co_3O_4 nanorod
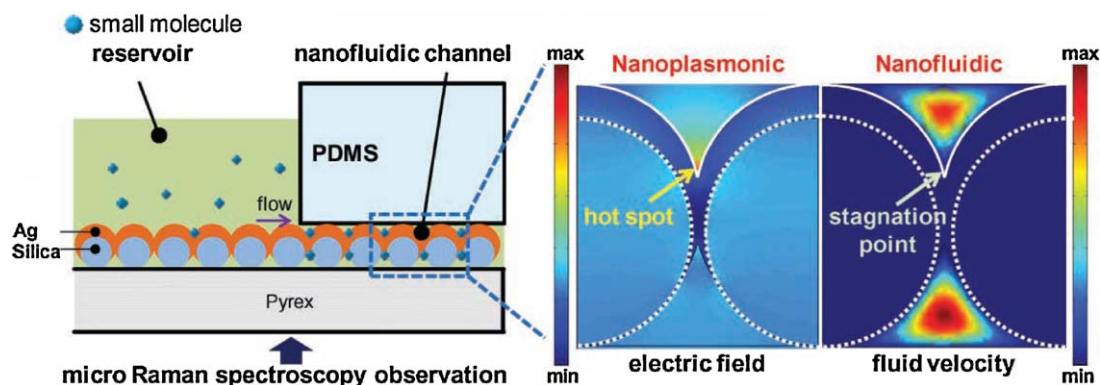
Figure 9 SERS enhancement of small molecules spatially entrapped near electromagnetic hot spots by using nanofluidic channels with localized SPR.
Reprinted with permission from Ref. [115]. Copyright 2011 Wiley-VCH Verlag GmbH & Co. KGaA.

arrays demonstrated stable superhydrophilicity without UV irradiation even after half a year owing to the improved roughness of the hierarchical structure and the abundant OH^- groups induced by the PLD and annealing processes [117].

Besides unique wettability properties, the surface-patterned nanostructures can also exhibit the relevant properties, such as self-clean, antifog, and fouling/anti-fouling. In particular, by MCC-assisted microcontact printing, bio-inspired creation of superhydrophobic compound-eye-like microstructures consisting of arrays of micro-hemispheres covered with nipple-like nanospheres, which exhibited profound antifog properties, were fabricated (Fig. 10) [118]. Since the adhesive force of dust particles to rough micro- and nanostructures is far less than that of the particles with spherical beads, fog drops may take the particles away from the superhydrophobic eye surface, thereby achieving cleaning in a humid habitat even though the particles are pervasive in the air. Moreover, flexible polymer surfaces with a nanofibrillar structured surface were fabricated by a novel approach combining colloidal lithography, silicon etching, and nanomolding technology [119]. The as-prepared artificial surface featured densely packed polymeric nanofibers with super-hydrophobic, water-repellent, and ''easy-to-clean'' characteristics.

Biological and chemical sensing

2D patterned nanostructures based on MCCs can be employed as sensitive sensors for detecting small molecules and biological macromolecules via different mechanisms, such as SERS-based, SPR-based, and photonic crystal-based sensors. Since the SERS-based sensing has been described above (SERS section), this part will focus on the SPR-based and photonic crystal-based sensing for the 2D patterned nanostructures obtained from MCCs.

It is known that SPR instruments are highly sensitive to the changes in refractive index near a metal surface, which could be used as chemical and biosensing without the need for fluorescent labels. Up till now, SPR- based chemical and biosensing have been realized for plenty of 2D patterned nanostructures based on MCCs. For instance,

Van Duyne and co-workers fabricated Ag particle arrays by deposition assisted by MCC masks, which exhibited sensitive response to the adsorption of Concanavalin A on the surface of Ag nanosensor functionalized with mannose [120]. Pt nanodisk arrays fabricated by hole-mask lithography assisted by MCCs were employed as an SPR-based sensor for detecting H_2 by monitoring the hydrogen-induced electronic changes in the system with the LSPR as a ''signal transducer'' [121].

Recently, we fabricated an SPR-based sensor using 2DOM Ag thin films obtained by nanosphere lithography at the gas/liquid interface, which were used for detecting both small molecules and biological macromolecules [92]. The preparation procedure for the 2DOM Ag thin film biosensor used for the detection of avidin via the specific binding between biotin and avidin is schematically shown in Fig. 11a. In the preparation procedure, the functionalization of the Ag surface with biotinylated bovine serum albumin (biotin-LC-BSA) was a crucial step to activate the thin film, that is, to render the biosensor high specificity to avidinanalyte. After removal of physically adsorbed biotin-LC-BSA with water, the Ag thin film could be considered as chemically modified with an SAM of biotin-LC-BSA molecules (namely, activated) and could be used to detect avidin molecules in solution. After the Ag thin film was immersed in avidin solution, the biotin groups on the Ag surface captured the avidin molecules to form biotin—avidin bindings to immobilize them on the Ag surface. The relationship between the reflectivity dip shift due to the specific adsorption of avidin molecules and the avidin concentration in solution was investigated. The reflectance spectra of the thin film biosensors at different states is shown in Fig. 11b, which suggests that after modification with biotin-LC-BSA, the original reflectivity dip of the unmodified Ag film at 440 nm slightly red-shifted to 442 nm, resulting from the replacement of air with biotin-LC-BSA SAMs. Fig. 11c shows the concentration dependence of the red shifts in reflectivity minimum at avidin concentrations lower than 400 pM. These results suggest that the 2DOM Ag thin film biosensors exhibited excellent performance with low detection limit (<100 pM) and broad working range (100 pM to 200 nM), indicating that they may be a promising candidate for high-performance biosensors.
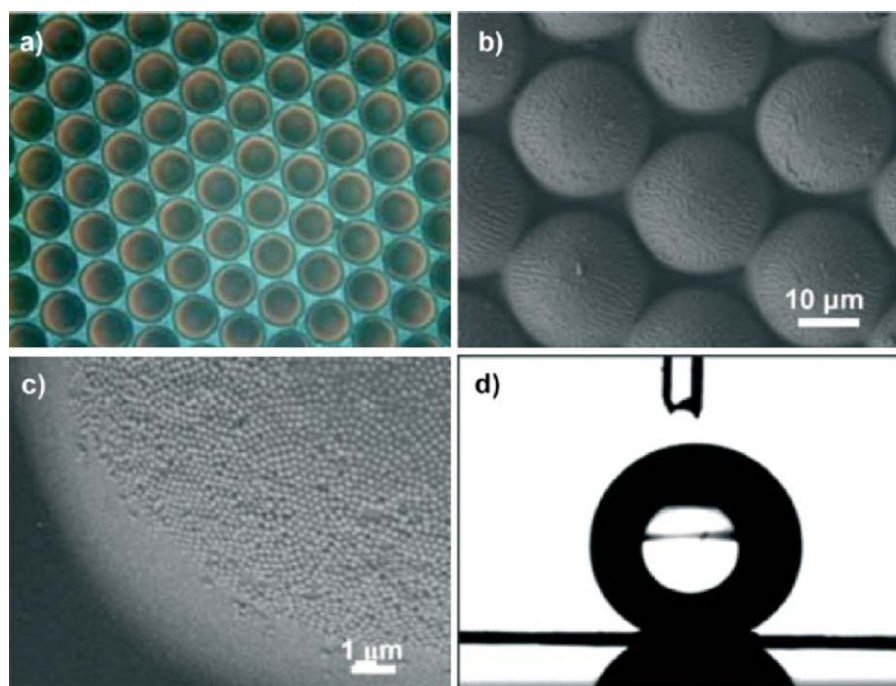
Figure 10 (a) Optical microscope image of artificial compound-eye analogues. (b, c) SEM images of hcp PDMS micro-hemispheres and silica nanospheres mimicking the microstructures of mosquito compound eyes. (d) A spherical water droplet on the artificial compound-eye surface.
Reprinted with permission from Ref. [118]. Copyright 2007 Wiley-VCH Verlag GmbH & Co. KGaA.

In the SPR-based molecular sensing with 2D patterned nanostructures based on MCCs, the chemical sensitivity relied on refractive index changes that shift plasmon resonances to monitor the analyte. However, more attractive approaches to chemical sensing would use methods that allow the visual determination of the chemical species and their concentrations. Recently, Asher and co-workers developed the first high-diffraction efficiency 2D photonic crystals for molecular recognition and chemical sensing applications [122]. The fabrication process of the 2D photonic crystal for sensing applications is illustrated in Fig. 12a. First, a water/propanol PS particle dispersion is dropped onto a Hg surface. Then, the dispersion spreads to form a 2D close-packed PS particle array as the solvent evaporates. A hydrogel film is polymerized around the 2D array and then the swelled hydrogel with the embedded 2D array is peeled from the glass substrate. Finally, the diffraction from the 2D array/hydrogel sandwich is monitored visually. The visually evident diffraction color of the 2D array is altered because the hydrogel network swells or shrinks in response to analyte concentration changes. These 2D photonic crystals exhibit ultrahigh diffraction efficiencies that enable them to be used for visual determination of analyte concentrations. Fig. 12b clearly shows the visually evident color changes that occur with changing pH values.

Solar cells

The periodic nanostructure arrays fabricated with the assistance of MCCs show promising applications in fabricating solar cells with enhanced performance. Up to now, several solar cells with specifically designed structures have been fabricated with the assistance of MCCs, aiming at improving efficiency through increasing light absorbance. For instance, Garnett and Yang fabricated large-area silicon nanowire radial p−n junction photovoltaics by MCC-assisted etching [48]. The as-prepared structures exhibited profound antireflection properties, which considerably increased the path length of incident solar radiation. It was demonstrated that the nanowire arrays with proper lengths showed enhanced efficiencies compared with planar structures.

In addition to nanowire arrays, nanodome a-Si:H solar cell structure with effective antireflection and light trapping over a broad spectral range and a wide set of incidence angles was fabricated by depositing multilayer of different materials on nanocone substrates recently [123]. As illustrated in Fig. 13a, the multilayer consisted of 100 nm thick Ag as a back reflector, 80 nm thick transparent conducting oxide (TCO) as both bottom and top electrode, and a thin a-Si:H active layer of 280 nm (from top to bottom: p−i−n, 10−250−20 nm). The SEM images of the initial nanocone quartz substrate and the obtained nanodome a-Si:H solar cell are shown in Fig. 13b and c, respectively. The nanodome devices look black due to efficient antireflection and light trapping, while the flat film devices are mirror-like, highly reflective, and look red because of inefficient light absorption at the long wavelength (Fig. 13d). The nanodome device exhibits a power efficiency of 5.9% while the flat device exhibits an efficiency of 4.7%, as shown in Fig. 13e.

Recently, a new concept for light trapping in thin film solar cells through the use of wavelength-scale
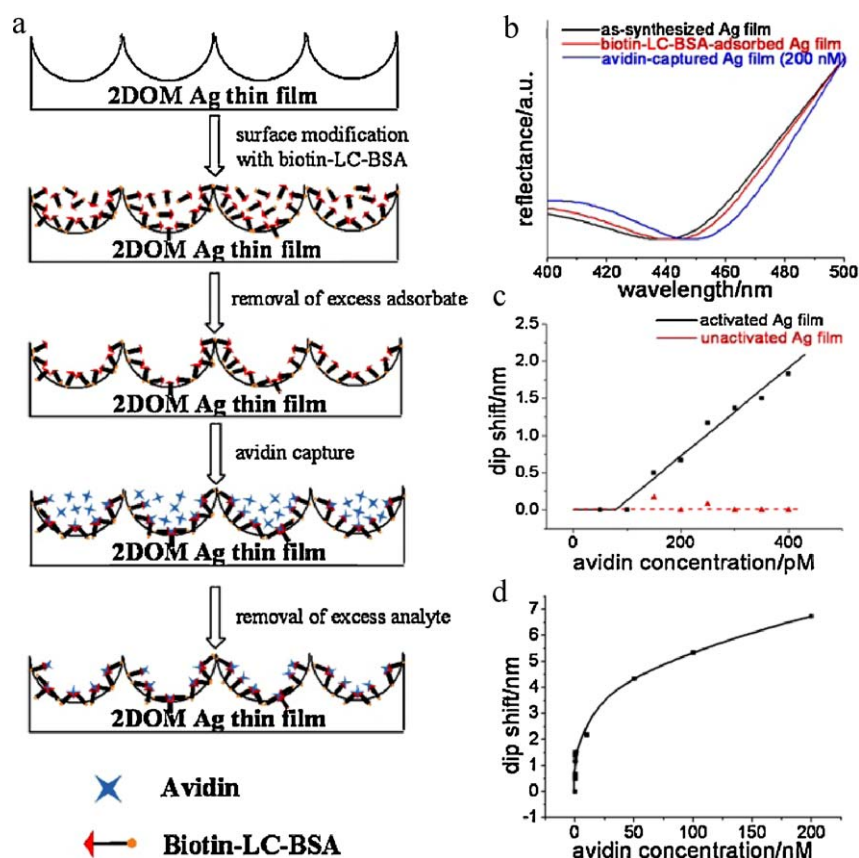
Figure 11 (a) Procedure for the preparation and operation of biosensor based on 2DOM Ag film for the detection of avidin molecules. (b) Reflectance spectra of 2DOM Ag thin film biosensors with different adsorbed molecules. (c, d) Relationship between the reflectivity dip position and the avidin concentration in the concentration range of 0—400 pM (c) and the range of 0—200 nm (d). Reprinted with permission from Ref. [92]. Copyright 2010 Wiley-VCH Verlag GmbH & Co. KGaA.

resonant dielectric nanospheres that support whispering gallery modes was adopted to enhance absorption and photocurrent [124]. By assembling MCCs of resonant silica nanospheres atop an a-Si layer, several photovoltaic absorber configurations were investigated and it was demonstrated that strong whispering gallery modes can significantly increase light absorption in a-Si thin-film solar cells.

In addition, quasi-ordered hollow TiO_2 hemispheres prepared by MCC-assisted gas/solid deposition were proved useful for dye-sensitized solar energy applications [125]. Because of the hollow structure that could promote electron transport and the large surface area that could enhance dye loading, the as-prepared hollow TiO_2 hemisphere arrays exhibited an enhanced photo-conversion efficiency (3.49%).

Photocatalysis

Photocatalysis plays an important role in environmental protection and energy conversion and hence great efforts have been made to synthesize nanostructured photocatalysts with high specific surface area aiming at improving the performance of photocatalysis. Hierarchal periodic structures fabricated with the assistance of MCCs may exhibit enhanced photocatalysis properties. For instance, Koshizaki and co-workers fabricated hierarchical amorphous TiO_2

hcp nanocolumn arrays by depositing amorphous TiO_2 on nanospheres of MCCs [126]. The photocatalysis performance of the as-prepared structures was clearly the best compared to anatase TiO_2 nanocolumn arrays and amorphous TiO_2 films. The reason why the amorphous hcp nanocolumn array exhibited better photocatalysis performance than that of an anatase nanocolumn array is the possession of much higher specific surface area originated from porous structures. Besides, an ordered structured nanocolumn array of amorphous TiO_2 can enhance photocatalytic activity better than an amorphous TiO_2 thin film, which may be ascribed to the special hierarchical structures composed of radiation-shaped nanobranches emanating from a center point on the PS sphere. In addition, a TiO_2 film/Cu_2O microgrid heterojunction was prepared by depositing a Cu_2O microgrid on the surface of a TiO_2 film with the assistance of MCCs [127]. The coupled system in this configuration showed higher photocatalytic activity under solar light irradiation than Cu_2O and TiO_2 films.

Field emission

Field-emission (FE) properties are of great commercial interest in flat-panel displays and other microelectronic devices. Recently, researchers have found that cathodes made of periodic regular arrays are very helpful for producing a
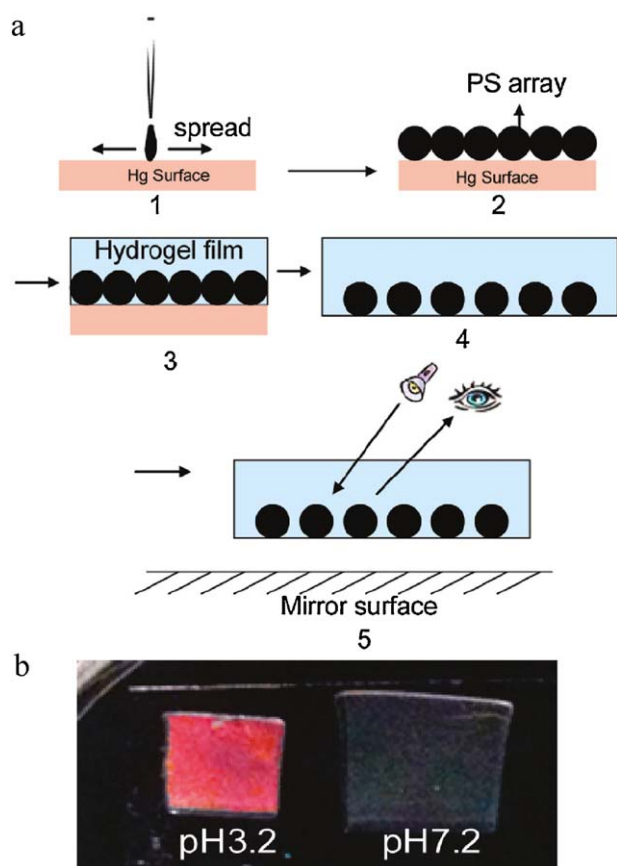
Figure 12 (a) Fabrication of a 2-D photonic crystal for sensing applications. (b) Optical photograph showing the 2D PS array/hydrogel-diffracted colors at pH 3.2 and 7.2.
Reprinted with permission from Ref. [122]. Copyright 2011 American Chemical Society.

low operating voltage and a fairly stable current because of the elimination of the shield effect on densely packed one-dimensional (1D) nanostructure arrays in field emission. Thus, much attention has been paid to the design of FE cathodes made of periodic or patterned arrays. By using MCCs as templates, various periodic 1D nanostructure arrays of semiconductors with tunable FE properties have been fabricated. As described above, periodic anatase TiO_2 nanorod arrays were fabricated through the PLD process by utilizing PS MCCs as templates, which was followed by annealing in air [66]. By tuning the nanosphere size and the background gas pressure applied during the PLD process, it was concluded that the hexagonal nonclose-packed nanorod arrays with the smallest periodicity and the largest distance between adjacent nanorods exhibited the best FE properties. Furthermore, template deformation-tailored ZnO nanorod/nanowire arrays were also used to investigate the pattern-dependent FE properties [71]. The NR/NW density, uniformity, and tapering were all adjusted through selection of template size and deformation, and electrolyte composition. In line with the adjustments, the field emission performance of the arrays was significantly improved. These results are highly attractive for developing next-generation field emitters based on the periodic arrays.
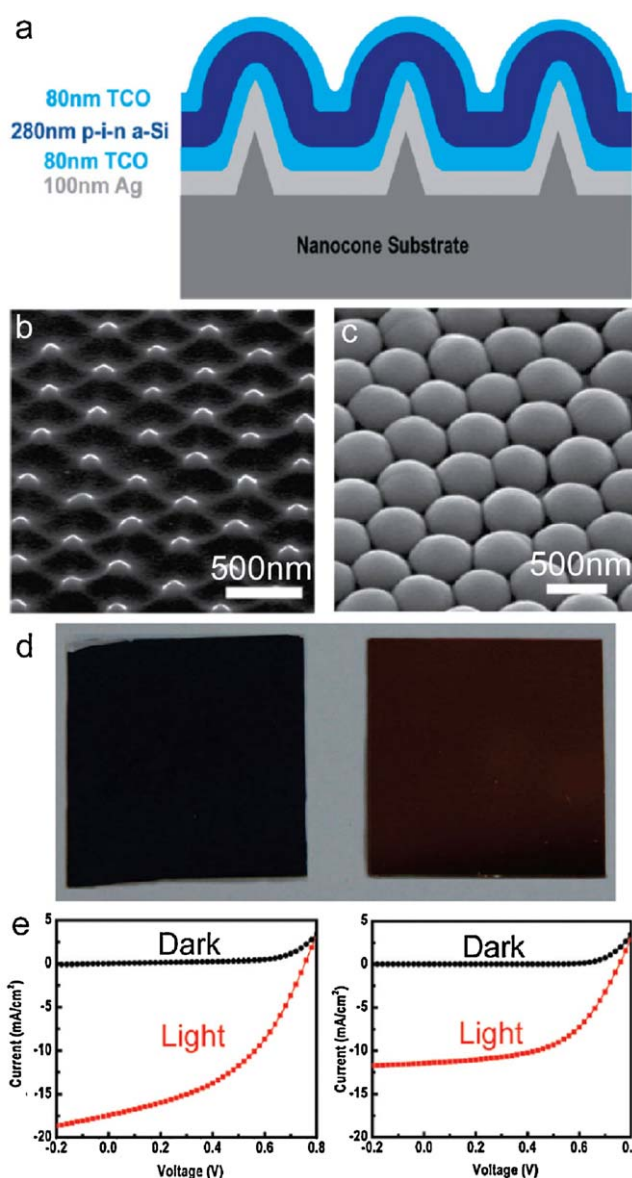
Figure 13 (a) Schematic showing the cross-sectional structure of nanodome solar cells. SEM images taken at 45° on (b) nanocone quartz substrate and (c) a-Si:H nanodome solar cells after deposition of multilayers of materials on nanocones. (d) Photographs of nanodome solar cells (left) and flat film solar cells (right). (e) Dark and light $I–V$ curve of solar cell devices for nanodomes (left) and flat substrates (right).
Reprinted with permission from Ref. [123]. Copyright 2010 American Chemical Society.

Biomimetic synthesis

MCCs can be applied as typical 2D periodic templates for the biomimetic synthesis of artificial structures that mimic some natural 2D periodic structures found in living organisms. Actually, the bio-inspired fabrication of superhydrophobic compound-eye-like microstructures consisting of arrays of micro-hemispheres covered with nipple-like nanospheres already provided a good example for the biomimetic synthesis [118]. Here we give two additional examples of
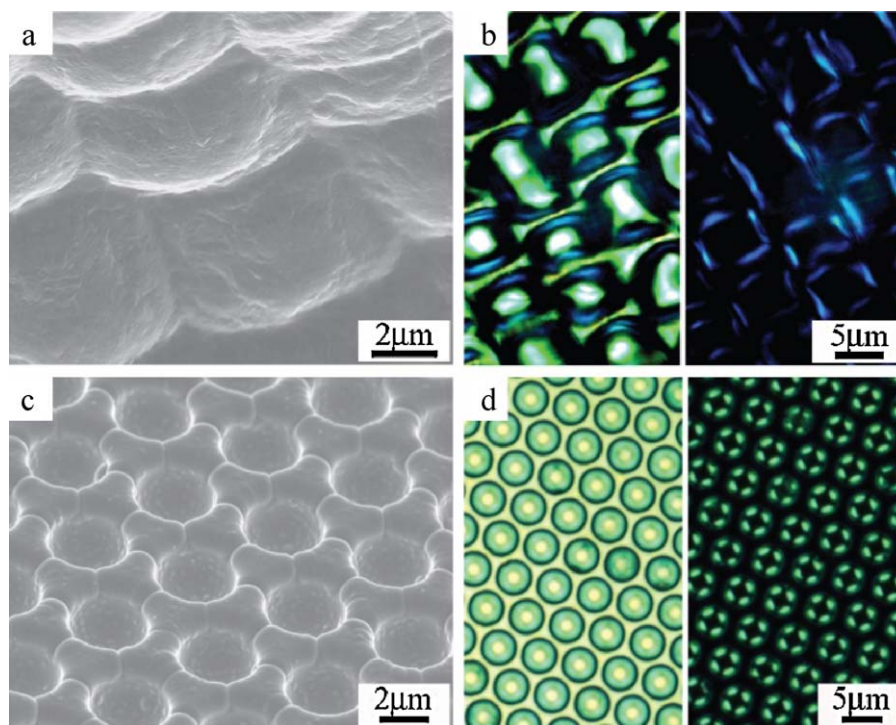
Figure 14   Natural photonic structure of the bright green wings of the *P. blumei* butterfly: (a) SEM image, (b) optical micrographs (left) and optical micrograph with crossed polarizers (right). Artificial optical mimic structure of concavities covered by a conformal multilayer stack of 11 alternating layers of titania and alumina: (c) SEM image, (d) optical micrograph (left) and optical micrograph with crossed polarizers (right).
Reprinted with permission from Ref. [131]. Copyright 2010 Macmillan Publishers Ltd.

biomimetic synthesis, namely, the fabrication of structures that mimic microlens arrays in brittlestar and wing scale structures of butterfly.

Microlens arrays are found in some living organisms such as brittlestars and they function as optical systems in addition to the mechanical function as exterior skeletons [128]. The fabrication of biomimetic microlens arrays with integrated pores, whose appearance and function are similar to highly efficient optical elements formed by brittlestars, has attracted great interest [129]. Among the variety of techniques developed to fabricate microlens arrays, methods based on MCCs have been proved feasible. For instance, Xia and co-workers developed a self-assembly approach based on physical confinement and successfully fabricated microlens arrays with controllable optical parameters, as well as the fill factors and patterns [130]. While the microlens arrays discovered in nature are often made by single crystals of calcite, most of the artificial microlens arrays are made by polymers or soft hydrogels. It remains a challenge to realize the fabrication of microlens arrays made by calcite single crystals.

Recently, Steiner and co-workers successfully fabricated the periodic structures mimicking the colorful wing scale structure of the *Papilio blumei* butterfly with the assistance of MCCs [131]. In the wings of butterflies, a combination of multilayer interference, optical gratings, photonic crystals and other optical structures gives rise to complex color mixing. The SEM image shown in Fig. 14a suggests that the surface of a wing scale is covered with concavities that are arranged in ordered lines alone the scale. These concavities

are clad with a multilayer that reflects yellow-green light at their centers and blue at their edges (Fig. 14b, left). By observing the scales in an optical microscope with crossed polarizers, the yellow-green light is extinguished, but the blue light can still be detected along four segments of each edge (Fig. 14b, right). In order to create regularly arranged concavities of appropriate dimensions, and reproduce its multilayer structures and mimic the optical characteristics, MCCs were used as templates to electrochemically deposit platinum or gold into the interstitial space between the microspheres, creating a negative replica. Then, by atomic layer deposition, a multilayer consisting of 11 alternating titania and alumina layers were deposited on the negative replica, as shown in Fig. 14c. These particular layer thicknesses were chosen in an attempt to create a quarter-wave stack with a stop-band center wavelength in the green-yellow spectral range to match the reflectance band of the natural Papilio structure closely. Under a light microscope, the concavity edges appear turquoise, and the centers and interstitial regions are yellow (Fig. 14d, left). Between crossed polarizers only the green concavity edges are visible (Fig. 14d, right), indicating that the as-prepared structure mimicked the optical characteristics of the *P. blumei* butterfly.

Other applications

Besides all the above-mentioned applications, 2D patterned nanostructures obtained with the assistance of MCCs still

show great application potential in many other fields, including biological and electronic applications.

Membranes are used in many fields such as the pharmaceutical, biotechnological, and food industries for the removal of particles or bacteria, as well as for waste water purification. The fabrication of the free-standing polyethersulfone nanonet films with a high porosity with the assistance of MCCs opens a new route towards free-standing porous polymer membranes that may find important applications in separation and purification [53]. Moreover, MCC templates combined with selective surface modification provide an efficient and reliable route towards highly ordered protein patterns, which is of key importance across a number of chemically and biologically important applications including sensor development, proteomics and bioengineering [84–86]. Furthermore, a novel type of matrix with regular nanotopography composed of crosslinked carbon nanotubes was prepared using MCC templates and was used as a cell-growing scaffold for detailed investigation on its cytocompatibility and the interaction with human osteoblast cells [132].

Periodic graphene nanomeshes with narrow necks (<20 nm) were prepared by MCC-assisted etching and the resulting structures exhibited promising electronic properties featuring high conductivities and on-off ratios up to 10 [54]. The apparent advantages of the presented method are the possibilities of fabricating periodic graphene nanostructures with different periodicities, ranging from ~100 nm to several micrometers, and also varying the periodicity and the neck width independently. Besides, the MCC-based arrays of hemispherical nanowells with diameters as small as 50 nm can be used as zeptoliter reaction vessels for the preparation of simple inorganic salts and semiconducting nanocrystals [133]. In addition, MCCs can be employed for the fabrication of a variety of chemically functionalized Janus particles that possess controllable anisotropy (patchiness) with the aid of a masking/unmasking technique [134].

Conclusions and outlook

The MCC-based colloidal lithography has been demonstrated to be a facile, inexpensive, efficient, and flexible nanofabrication approaches towards various 2D patterned nanostructures with high controllability and reproducibility. As the prerequisite templates for colloidal lithography, MCCs can be routinely prepared by many self-assembly techniques. While the common hcp MCCs can be readily obtained by various interfacial self-assembly methods such as drop-coating, dip-coating, spin-coating, electrophoretic deposition, and self-assembly at the gas/liquid interface, complex MCCs (e.g., ncp MCCs and patterned MCCs) can be realized by many strategies including etching of hcp MCCs, spin-coating, electric-field-directed assembly, template-directed assembly, and transfer printing. In general, the MCC-based colloidal lithography can be realized by MCC-assisted fabrication including etching and deposition at different two-phase (e.g., gas/solid, liquid/solid, and gas/liquid) interfaces and by MCC-assisted assembly from preformed nanoscale building blocks. Upon deliberate combination between MCC templates with adjustable structural parameters and sophisticated fabrication and assembly techniques result in a great flexibility in tuning the structural parameters (e.g., feature size, shape, orientation, mutual distance, periodicity, and arrangement) of the final patterned nanostructures, as well as their chemical composition and materials properties. Till now, the MCC-based colloidal lithography techniques have been successfully used for the controllable fabrication and assembly of a wide variety of 2D patterned nanostructures, such as 2D periodic arrays of various nano-objects (e.g., nanoparticles, nanotips, nanowires, nanobowls, nanovoids, nanorings, and nanocrescents), and freestanding nanonet films or nanoporous membranes. It has been demonstrated that the 2D patterned nanostructures based on MCCs show great potential applications in many important areas, such as photonics, plasmonics, SERS, antireflection, surface wetting, biological and chemical sensing, solar cells, photocatalysis, field emission, biomimetic fabrication, and other biological and electronic applications.

Despite the exciting developments in the controllable fabrication, assembly, and applications of 2D patterned nanostructures based on MCCs, many challenges still remain ahead: (1) Assembly of desirable MCC templates. The facile and reproducible fabrication of defect-free MCCs in a large area is a long-term goal to pursue in the area of colloid crystallization. Meanwhile, it is highly desirable to develop effective methods to assemble small colloidal nanospheres (<100 nm) into high-quality MCCs. Moreover, it is worthwhile to explore the controllable assembly of MCCs with more complex patterns, such as MCCs made of nonspherical particles or multiple components. (2) MCC-assisted fabrication and assembly. It is challenging to fabricate 2D patterned nanostructures with arbitrarily adjustable structural parameters and chemical compositions through original and rational design of the MCC-assisted fabrication and assembly strategies. It is also desirable to realize the preparation of 2D patterned nanostructures with even more complex patterns, such as 2D arrays of nanostructured units with tunable shapes, 2D patterned hybrid nanostructures, and hierarchical 2D nanostructures with 3D features. It is also demanding to optimize some of the time-consuming fabrication techniques associated with expensive equipments and to develop alternative time-effective and low-cost fabrication techniques. (3) Applications of MCC-based nanostructures. Although many applications of MCC-based nanostructures have been demonstrated, the relationship between the application performance and the structural parameters of the patterned nanostructures remains unclear in many cases. Great efforts are needed to investigate the pattern-dependent properties and application performance so as rationally design 2D patterned nanostructures with optimized structural parameters for specific applications. Finally, the applications related to energy conversion and storage and the biological and biomedical applications are expected to receive increasing attentions for the MCC-based functional nanostructures.

Acknowledgments

References

[1] J. Henzie, J.E. Barton, C.L. Stender, T.W. Odom, Acc. Chem. Res. 39 (2006) 249.

[2] Y. Lei, S. Yang, M. Wu, G. Wilde, Chem. Soc. Rev. 40 (2011) 1247.

[3] B.D. Gates, Q.B. Xu, M. Stewart, D. Ryan, C.G. Willson, G.M. Whitesides, Chem. Rev. 105 (2005) 1171.

[4] M. Geissler, Y. Xia, Adv. Mater. 16 (2004) 1249.

[5] D. Wouters, U.S. Schubert, Angew. Chem. Int. Ed. 43 (2004) 2480.

[6] K. Salaita, Y. Wang, C.A. Mirkin, Nat. Nanotechnol. 2 (2007) 145.

[7] L.J. Guo, Adv. Mater. 19 (2007) 495.

[8] A. Perl, D.N. Reinhoudt, J. Huskens, Adv. Mater. 21 (2009) 2257.

[9] S.M. Yang, S.G. Jang, D.G. Choi, S. Kim, H.K. Yu, Small 2 (2006) 458.

[10] G. Zhang, D. Wang, Chem. Asian J. 4 (2009) 236.

[11] J. Zhang, Y. Li, X. Zhang, B. Yang, Adv. Mater. 22 (2010) 4249.

[12] Y. Li, W. Cai, G. Duan, Chem. Mater. 20 (2008) 615.

[13] Y. Li, N. Koshizakib, W. Cai, Coord. Chem. Rev. 255 (2011) 357.

[14] L. Li, T. Zhai, H. Zeng, X. Fang, Y. Bando, D. Golberg, J. Mater. Chem. 21 (2011) 40.

[15] S. Yang, Y. Lei, Nanoscale 3 (2011) 2768.

[16] F. Marlow, Muldarisnur, P. Sharifi, R. Brinkmann, C. Mendive, Angew. Chem. Int. Ed. 48 (2009) 6212.

[17] J.H. Moon, S. Yang, Chem. Rev. 110 (2010) 547.

[18] C.I. Aguirre, E. Reguera, A. Stein, Adv. Funct. Mater. 20 (2010) 2565.

[19] J. Ge, Y. Yin, Angew. Chem. Int. Ed. 50 (2011) 1492.

[20] J. Wang, Y. Zhang, S. Wang, Y. Song, L. Jiang, Acc. Chem. Res. 44 (2011) 405.

[21] U.C. Fischer, H.P. Zingsheim, J. Vac. Sci. Technol. 19 (1981) 881.

[22] H.W. Deckman, J.H. Dunsmuir, Appl. Phys. Lett. 41 (1982) 377.

[23] J.C. Hulteen, R.P. Van Duyne, J. Vac. Sci. Technol. A 13 (1995) 1553.

[24] C.L. Haynes, R.P. Van Duyne, J. Phys. Chem. B 105 (2001) 5599.

[25] Y.N. Xia, B. Gates, Y.D. Yin, Y. Lu, Adv. Mater. 12 (2000) 693.

[26] N.D. Denkov, O.D. Velev, P.A. Kralchevsky, I.B. Ivanov, H. Yoshimura, K. Nagayama, Langmuir 8 (1992) 3183.

[27] A.S. Dimitrov, K. Nagayama, Langmuir 12 (1996) 1303.

[28] X. Li, T.Q. Wang, J.H. Zhang, X. Yan, X.M. Zhang, D.F. Zhu, W. Li, X. Zhang, B. Yang, Langmuir 26 (2010) 2930.

[29] P. Jiang, M.J. McFarland, J. Am. Chem. Soc. 126 (2004) 13778.

[30] M. Trau, D.A. Saville, I.A. Aksay, Science 272 (1996) 706.

[31] S.O. Lumsdon, E.W. Kaler, O.D. Velev, Langmuir 20 (2004) 2108.

[32] M. Bardosova, M.E. Pemble, I.M. Povey, R.H. Tredgold, Adv. Mater. 22 (2010) 3104.

[33] C. Li, G. Hong, P. Wang, D. Yu, L. Qi, Chem. Mater. 21 (2009) 891.

[34] A. Plettl, F. Enderle, M. Saitner, A. Manzke, C. Pfahler, S. Wiedemann, P. Ziemann, Adv. Funct. Mater. 19 (2009) 3279.

[35] P. Jiang, T. Prasad, M.J. McFarland, V.L. Colvin, Appl. Phys. Lett. 89 (2006) 011908.

[36] Y. Liu, R.G. Xie, X.Y. Liu, Appl. Phys. Lett. 91 (2007) 063105.

[37] X. Yan, J.M. Yao, G.A. Lu, X. Chen, K. Zhang, B. Yang, J. Am. Chem. Soc. 126 (2004) 10510.

[38] X. Yan, J.M. Yao, G. Lu, X. Li, J.H. Zhang, K. Han, B. Yang, J. Am. Chem. Soc. 127 (2005) 7688.

[39] N.N. Khanh, K.B. Yoon, J. Am. Chem. Soc. 131 (2009) 14228.

[40] P. Maury, M. Escalante, D.N. Reinhoudt, J. Huskens, Adv. Mater. 17 (2005) 2718.

[41] M.H.S. Shyr, D.P. Wernette, P. Wiltzius, Y. Lu, P.V. Braun, J. Am. Chem. Soc. 130 (2008) 8234.

[42] K.P. Velikov, C.G. Christova, R.P.A. Dullens, A. van Blaaderen, Science 296 (2002) 106.

[43] D.Y. Wang, H. Mohwald, Adv. Mater. 16 (2004) 244.

[44] M.H. Kim, S.H. Im, O.O. Park, Adv. Mater. 17 (2005) 2501.

[45] Z.C. Zhou, Q.F. Yan, Q. Li, X.S. Zhao, Langmuir 23 (2007) 1473.

[46] V. Kitaev, G.A. Ozin, Adv. Mater. 15 (2003) 75.

[47] J. Yu, Q.F. Yan, D.Z. Shen, ACS Appl. Mater. Interface 2 (2010) 1922.

[48] E. Garnett, P.D. Yang, Nano Lett. 10 (2010) 1082.

[49] J. Zhu, Z.F. Yu, G.F. Burkhard, C.M. Hsu, S.T. Connor, Y.Q. Xu, Q. Wang, M. McGehee, S.H. Fan, Y. Cui, Nano Lett. 9 (2009) 279.

[50] C.H. Sun, W.L. Min, P. Jiang, Chem. Commun. (2008) 3163.

[51] A.V. Whitney, B.D. Myers, R.P. Van Duyne, Nano Lett. 4 (2004) 1507.

[52] Y. Li, E.J. Lee, W. Cai, K.Y. Kim, S.O. Cho, ACS Nano 2 (2008) 1108.

[53] C. Acikgoz, X.Y. Ling, I.Y. Phang, M.A. Hempenius, D.N. Reinhoudt, J. Huskens, C.J. Vancso, Adv. Mater. 21 (2009) 2064.

[54] A. Sinitskii, J.M. Tour, J. Am. Chem. Soc. 132 (2010) 14730.

[55] L. Liu, Y. Zhang, W. Wang, C. Gu, X. Bai, E. Wang, Adv. Mater. 23 (2011) 1246.

[56] Z.P. Huang, H. Fang, J. Zhu, Adv. Mater. 19 (2007) 744.

[57] K.Q. Peng, M.L. Zhang, A.J. Lu, N.B. Wong, R.Q. Zhang, S.T. Lee, Appl. Phys. Lett. 90 (2007) 163123.

[58] J.M. McLellan, M. Geissler, Y.N. Xia, J. Am. Chem. Soc. 126 (2004) 10830.

[59] F. Sun, W. Cai, Y. Li, G. Duan, W.T. Nichols, C. Liang, N. Koshizaki, Q. Fang, I.W. Boyd, Appl. Phys. B: Lasers Opt. 81 (2005) 765.

[60] M. Bechelany, X. Maeder, J. Riesterer, J. Hankache, D. Lerose, S. Christiansen, J. Michler, L. Philippe, Cryst. Growth Des. 10 (2010) 587.

[61] C.L. Haynes, A.D. McFarland, M.T. Smith, J.C. Hulteen, R.P. Van Duyne, J. Phys. Chem. B 106 (2002) 1898.

[62] M.C. Gwinner, E. Koroknay, L.W. Fu, P. Patoka, W. Kandulski, M. Giersig, H. Giessen, Small 5 (2009) 400.

[63] M. Retsch, M. Tamm, N. Bocchio, N. Horn, R. Forch, U. Jonas, M. Kreiter, Small 5 (2009) 2105.

[64] G. Zhang, D.Y. Wang, H. Mohwald, Nano Lett. 7 (2007) 127.

[65] I.D. Kim, A. Rothschild, T. Hyodo, H.L. Tuller, Nano Lett. 6 (2006) 193.

[66] Y. Li, X.S. Fang, N. Koshizaki, T. Sasaki, L. Li, S.Y. Gao, Y. Shimizu, Y. Bando, D. Golberg, Adv. Funct. Mater. 19 (2009) 2467.

[67] K. Kempa, B. Kimball, J. Rybczynski, Z.P. Huang, P.F. Wu, D. Steeves, M. Sennett, M. Giersig, D. Rao, D.L. Carnahan, D.Z. Wang, J.Y. Lao, W.Z. Li, Z.F. Ren, Nano Lett. 3 (2003) 13.

[68] K.C. Hsieh, T.Y. Tsai, D.H. Wan, H.L. Chen, N.H. Tai, ACS Nano 4 (2010) 1327.

[69] B. Fuhrmann, H.S. Leipner, H.R. Hoche, L. Schubert, P. Werner, U. Gosele, Nano Lett. 5 (2005) 2524.

[70] X.X. Zhang, D.F. Liu, L.H. Zhang, W.L. Li, M. Gao, W.J. Ma, Y. Ren, Q.S. Zeng, Z.Q. Niu, W.Y. Zhou, S.S. Xie, J. Mater. Chem. 19 (2009) 962.

[71] H.B. Zeng, X.J. Xu, Y. Bando, U.K. Gautam, T.Y. Zhai, X.S. Fang, B.D. Liu, D. Golberg, Adv. Funct. Mater. 19 (2009) 3165.

[72] J. Elias, C. Levy-Clement, M. Bechelany, J. Michler, G.Y. Wang, Z. Wang, L. Philippe, Adv. Mater. 22 (2010) 1607.

[73] S.K. Yang, W.P. Cai, L.C. Kong, Y. Lei, Adv. Funct. Mater. 20 (2010) 2527.

[74] G. Duan, W. Cai, Y. Luo, F. Sun, Adv. Funct. Mater. 17 (2007) 644.

[75] W. Dong, H. Dong, Z.L. Wang, P. Zhan, Z.Q. Yu, X.N. Zhao, Y.Y. Zhu, N.B. Ming, Adv. Mater. 18 (2006) 755.

[76] W. Ahn, D.K. Roper, ACS Nano 4 (2010) 4181.

[77] F.Q. Sun, W.P. Cai, Y. Li, B.Q. Cao, Y. Lei, L.D. Zhang, Adv. Funct. Mater. 14 (2004) 283.

[78] L.C. Jia, W.P. Cai, H.Q. Wang, F.Q. Sun, Y. Li, ACS Nano 3 (2009) 2697.

[79] D. Lan, Y.R. Wang, X.L. Du, Z.X. Mei, Q.K. Xue, K. Wang, X.D. Han, Z. Zhang, Cryst. Growth Des. 8 (2008) 2912.

[80] H.J. Nam, D.Y. Jung, G.R. Yi, H. Choi, Langmuir 22 (2006) 7358.

[81] T.Q. Wang, X. Li, J.H. Zhang, Z.Y. Ren, X.M. Zhang, X. Zhang, D.F. Zhu, Z.H. Wang, F. Han, X.Z. Wang, B. Yang, J. Mater. Chem. 20 (2010) 152.

[82] Z.Q. Sun, Y. Li, J.H. Zhang, Y.F. Li, Z.H. Zhao, K. Zhang, G. Zhang, J.R. Guo, B. Yang, Adv. Funct. Mater. 18 (2008) 4036.

[83] R.B. Pernites, E.L. Foster, M.J.L. Felipe, M. Robinson, R.C. Advincula, Adv. Mater. 23 (2011) 1287.

[84] G.M.L. Messina, C. Satriano, G. Marletta, Chem. Commun. (2008) 5031.

[85] G. Singh, H.J. Griesser, K. Bremmell, P. Kingshott, Adv. Funct. Mater. 21 (2011) 540.

[86] G. Singh, S. Pillai, A. Arpanaei, P. Kingshott, Adv. Mater. 23 (2011) 1519.

[87] H. Xu, W.A. Goedel, Angew. Chem. Int. Ed. 42 (2003) 4694.

[88] F. Yan, W.A. Goedel, Nano Lett. 4 (2004) 1193.

[89] J.Y. Chen, D.M. Chao, X.F. Lu, W.J. Zhang, S.K. Manohar, Macromol. Rapid Commun. 27 (2006) 771.

[90] F.Q. Sun, J.C. Yu, Angew. Chem. Int. Ed. 46 (2007) 773.

[91] C. Li, G. Hong, L. Qi, Chem. Mater. 22 (2010) 476.

[92] G. Hong, C. Li, L. Qi, Adv. Funct. Mater. 20 (2010) 3774.

[93] C. Li, G. Hong, H. Yu, L. Qi, Chem. Mater. 22 (2010) 3206.

[94] L. Qi, Coord. Chem. Rev. 254 (2010) 1054.

[95] J. Pacifico, D. Gomez, P. Mulvaney, Adv. Mater. 17 (2005) 415.

[96] J.X. Chen, W.S. Liao, X. Chen, T.L. Yang, S.E. Wark, D.H. Son, J.D. Batteas, P.S. Cremer, ACS Nano 3 (2009) 173.

[97] M.H. Kim, J.Y. Choi, H.K. Choi, S.M. Yoon, O.O. Park, D.K. Yi, S.J. Choi, H.J. Shin, Adv. Mater. 20 (2008) 457.

[98] S. Motavas, B. Omrane, C. Papadopoulos, Langmuir 25 (2009) 4655.

[99] T. Huang, Q. Zhao, J. Xiao, L. Qi, ACS Nano 4 (2010) 4707.

[100] H. Gao, W. Zhou, T.W. Odom, Adv. Funct. Mater. 20 (2010) 529.

[101] S.G. Romanov, A.V. Korovin, A. Regensburger, U. Peschel, Adv. Mater. 23 (2011) 2515.

[102] Y. Gao, A.D. Li, Z.B. Gu, Q.J. Wang, Y. Zhang, D. Wu, Y.F. Chen, N.B. Ming, S.X. Ouyang, T. Yu, Appl. Phys. Lett. 91 (2007) 031910.

[103] Y.F. Li, J.H. Zhang, B. Yang, Nano Today 5 (2010) 117.

[104] W.L. Min, B. Jiang, P. Jiang, Adv. Mater. 20 (2008) 3914.

[105] Y.F. Li, J.H. Zhang, S.J. Zhu, H.P. Dong, F. Jia, Z.H. Wang, Z.Q. Sun, L. Zhang, Y. Li, H.B. Li, W.Q. Xu, B. Yang, Adv. Mater. 21 (2009) 4731.

[106] J.M. Yao, A.P. Le, S.K. Gray, J.S. Moore, J.A. Rogers, R.G. Nuzzo, Adv. Mater. 22 (2010) 1102.

[107] J.A. Schuller, E.S. Barnard, W.S. Cai, Y.C. Jun, J.S. White, M.L. Brongersma, Nat. Mater. 9 (2010) 193.

[108] L.Y. Wu, B.M. Ross, L.P. Lee, Nano Lett. 9 (2009) 1956.

[109] P. Zhan, Z.L. Wang, H. Dong, J. Sun, J. Wu, H.T. Wang, S.N. Zhu, N.B. Ming, J. Zi, Adv. Mater. 18 (2006) 1612.

[110] X.L. Zhu, L. Shi, X.H. Liu, J. Zi, Z.L. Wang, Nano Res. 3 (2010) 807.

[111] M.D. Porter, R.J. Lipert, L.M. Siperko, G. Wang, R. Narayanana, Chem. Soc. Rev. 37 (2008) 1001.

[112] Y. Fang, N.H. Seong, D.D. Dlott, Science 321 (2008) 388.

[113] C. Farcau, S. Astilean, J. Phys. Chem. C 114 (2010) 11717.

[114] M.E. Abdelsalam, S. Mahajan, P.N. Bartlett, J.J. Baumberg, A.E. Russell, J. Am. Chem. Soc. 129 (2007) 7399.

[115] Y.-J. Oh, S.-G. Park, M.-H. Kang, J.-H. Choi, Y. Nam, K.-H. Jeong, Small 7 (2011) 184.

[116] Y. Li, W.P. Cai, B.Q. Cao, G.T. Duan, F.Q. Sun, C.C. Li, L.C. Jia, Nanotechnology 17 (2006) 238.

[117] L. Li, Y. Li, S.Y. Gao, N. Koshizaki, J. Mater. Chem. 19 (2009) 8366.

[118] X.F. Gao, X. Yan, X. Yao, L. Xu, K. Zhang, J.H. Zhang, B. Yang, L. Jiang, Adv. Mater. 19 (2007) 2213.

[119] T.S. Kustandi, V.D. Samper, D.K. Yi, W.S. Ng, P. Neuzil, W.X. Sun, Adv. Funct. Mater. 17 (2007) 2211.

[120] C.R. Yonzon, E. Jeoungf, S.L. Zou, G.C. Schatz, M. Mrksich, R.P. Van Duyne, J. Am. Chem. Soc. 126 (2004) 12669.

[121] C. Langhammer, I. Zoric, B. Kasemo, Nano Lett. 7 (2007) 3122.

[122] J.-T. Zhang, L. Wang, J. Luo, A. Tikhonov, N. Kornienko, S.A. Asher, J. Am. Chem. Soc. 133 (2011) 9152.

[123] J. Zhu, C.M. Hsu, Z.F. Yu, S.H. Fan, Y. Cui, Nano Lett. 10 (2010) 1979.

[124] J. Grandidier, D.M. Callahan, J.N. Munday, H.A. Atwater, Adv. Mater. 23 (2011) 1272.

[125] S.C. Yang, D.J. Yang, J. Kim, J.M. Hong, H.G. Kim, I.D. Kim, H. Lee, Adv. Mater. 20 (2008) 1059.

[126] Y. Li, T. Sasaki, Y. Shimizu, N. Koshizaki, J. Am. Chem. Soc. 130 (2008) 14755.

[127] J.Y. Zhang, H.L. Zhu, S.K. Zheng, F. Pan, T.M. Wang, ACS Appl. Mater. Interface 1 (2009) 2111.

[128] J. Aizenberg, A. Tkachenko, S. Weiner, L. Addadi, G. Hendler, Nature 412 (2001) 819.

[129] S. Yang, J. Aizenberg, Nano Today (2005) 40.

[130] Y. Lu, Y.D. Yin, Y.N. Xia, Adv. Mater. 13 (2001) 34.

[131] M. Kolle, P.M. Salgard-Cunha, M.R.J. Scherer, F.M. Huang, P. Vukusic, S. Mahajan, J.J. Baumberg, U. Steiner, Nat. Nanotechnol. 5 (2010) 511.

[132] I. Firkowska, E. Godehardt, M. Giersig, Adv. Funct. Mater. 18 (2008) 3765.

[133] J.E. Barton, T.W. Odom, Nano Lett. 4 (2004) 1525.

[134] X.Y. Ling, I.Y. Phang, C. Acikgoz, M.D. Yilmaz, M.A. Hempenius, G.J. Vancso, J. Huskens, Angew. Chem. Int. Ed. 48 (2009) 7677.

Xiaozhou Ye received her BSc degree in the field of polymer science and engineering from Sichuan University in 2009. Then, she joined Prof. Limin Qi's group at Peking University as a PhD student. Her current research interests focus on the fabrication and application of patterned nanostructures based on colloidal crystal templates.

Limin Qi received his PhD degree in Physical Chemistry from Peking University in 1998. He then went to the Max Planck Institute of Colloids and Interfaces to work on biomimetic mineralization as a postdoctoral fellow. In 2000, he joined the College of Chemistry at Peking University, where he has been a full professor since 2004. He is an editorial board member of *Chinese Journal of Chemistry* and *Chinese Science Bulletin*, and an advisory board member of *Advanced Functional Materials* and *ACS Applied Materials & Interfaces*. His current research interests involve the controlled synthesis and hierarchical assembly of functional micro- and nanostructures by colloidal chemical methods as well as bio-inspired approaches.